NAVAL
POSTGRADUATE
SCHOOL

MONTEREY, CALIFORNIA

THESIS

TRANSMISSION OF A DETONATION WAVE ACROSS A SUDDEN EXPANSION WITH VARYING MIXTURE COMPOSITION

by

Elizabeth J. Touse

December 2003

Thesis Advisor:	Christopher M. Brophy
Co-Advisor:	Jose O. Sinibaldi

Approved for public release; distribution is unlimited

THIS PAGE INTENTIONALLY LEFT BLANK

REPORT DOCUMENTATION PAGE			Form Approved OMB No. 0704-0188
Public reporting burden for this collection of information is estimated to average 1 hour per response, including the time for reviewing instruction, searching existing data sources, gathering and maintaining the data needed, and completing and reviewing the collection of information. Send comments regarding this burden estimate or any other aspect of this collection of information, including suggestions for reducing this burden, to Washington headquarters Services, Directorate for Information Operations and Reports, 1215 Jefferson Davis Highway, Suite 1204, Arlington, VA 22202-4302, and to the Office of Management and Budget, Paperwork Reduction Project (0704-0188) Washington DC 20503.			
1. AGENCY USE ONLY ***(Leave blank)***	**2. REPORT DATE** December 2003	**3. REPORT TYPE AND DATES COVERED** Master's Thesis	
4. TITLE AND SUBTITLE: Transmission of a Detonation Wave Across a Sudden Expansion with Varying Mixture Composition			**5. FUNDING NUMBERS** N0001403WR20159
6. AUTHOR(S) Elizabeth J. Touse			
7. PERFORMING ORGANIZATION NAME(S) AND ADDRESS(ES) Naval Postgraduate School Monterey, CA 93943-5000			**8. PERFORMING ORGANIZATION REPORT NUMBER**
9. SPONSORING /MONITORING AGENCY NAME(S) AND ADDRESS(ES) Office of Naval Research Ballston Tower One 800 N. Quincy Street Arlington, VA 22217-5660			**10. SPONSORING/MONITORING AGENCY REPORT NUMBER**
11. SUPPLEMENTARY NOTES The views expressed in this thesis are those of the author and do not reflect the official policy or position of the Department of Defense or the U.S. Government.			
12a. DISTRIBUTION / AVAILABILITY STATEMENT Approved for public release; distribution is unlimited.			**12b. DISTRIBUTION CODE**

13. ABSTRACT (maximum 200 words)

Detonation waves were examined in axisymmetric and two-dimensional test configurations to determine the limits at which a detonation will successfully initiate and diffract from a small initiator tube into a larger main combustor. Tests were conducted for various initiator-to-main combustor area ratios. Additionally, for each area ratio, the fuel-oxygen initiator mixture was diluted with various nitrogen concentrations attempting to approach the mass fraction of nitrogen in air (79%).

Results of the axisymmetric testing showed that with an expansion area ratio of 2.0, detonations began to fail to initiate in the initiator section with nitrogen dilution as low as 45%. Although, through constructive interference such as wall reflections and shock-shock interactions, a detonation wave initiated in the main combustor for up to 60% nitrogen dilution. Results of the two-dimensional testing showed that for area ratios of 1.33 to 2.67, detonation waves successfully transmitted for all nitrogen dilution cases, including 79%. For an area ratio of 4.0, detonation waves successfully transmitted with 65% nitrogen dilution but failed with 70% nitrogen dilution.

14. SUBJECT TERMS Pulse Detonation Engines, PDE, Detonation Diffraction			**15. NUMBER OF PAGES** 93
			16. PRICE CODE
17. SECURITY CLASSIFICATION OF REPORT Unclassified	**18. SECURITY CLASSIFICATION OF THIS PAGE** Unclassified	**19. SECURITY CLASSIFICATION OF ABSTRACT** Unclassified	**20. LIMITATION OF ABSTRACT** UL

NSN 7540-01-280-5500 Standard Form 298 (Rev. 2-89)
Prescribed by ANSI Std. 239-18

THIS PAGE INTENTIONALLY LEFT BLANK

Approved for public release; distribution is unlimited

TRANSMISSION OF A DETONATION WAVE ACROSS A SUDDEN EXPANSION WITH VARYING MIXTURE COMPOSITION

Elizabeth J. Touse
Lieutenant, United States Navy
B.S., United States Naval Academy, 1997

Submitted in partial fulfillment of the
requirements for the degree of

MASTER OF SCIENCE IN ASTRONAUTICAL ENGINEERING

from the

NAVAL POSTGRADUATE SCHOOL
December 2003

Author: Elizabeth J. Touse

Approved by: Christopher M. Brophy
Thesis Advisor

Jose O. Sinibaldi
Co-Advisor

Anthony J. Healey
Chairman, Department of Mechanical & Astronautical Engineering

THIS PAGE INTENTIONALLY LEFT BLANK

ABSTRACT

Detonation waves were examined in axisymmetric and two-dimensional test configurations to determine the limits at which a detonation will successfully initiate and diffract from a small initiator tube into a larger main combustor. Tests were conducted for various initiator-to-main combustor area ratios. Additionally, for each area ratio, the fuel-oxygen initiator mixture was diluted with various nitrogen concentrations attempting to approach the mass fraction of nitrogen in air (79%).

Results of the axisymmetric testing showed that with an expansion area ratio of 2.0, detonations began to fail to initiate in the initiator section with nitrogen dilution as low as 45%. Although, through constructive interference such as wall reflections and shock-shock interactions, a detonation wave initiated in the main combustor for up to 60% nitrogen dilution. Results of the two-dimensional testing showed that for area ratios of 1.33 to 2.67, detonation waves successfully transmitted for all nitrogen dilution cases, including 79%. For an area ratio of 4.0, detonation waves successfully transmitted with 65% nitrogen dilution but failed with 70% nitrogen dilution.

THIS PAGE INTENTIONALLY LEFT BLANK

TABLE OF CONTENTS

LIST OF FIGURES

LIST OF TABLES

THIS PAGE INTENTIONALLY LEFT BLANK

ACKNOWLEDGEMENTS

I would like to thank my thesis advisors, Professor Christopher Brophy and Professor Jose Sinibaldi for their countless hours of patient instruction and hands-on guidance during this study. Their expertise and dedication provided an outstanding learning experience in an interesting laboratory environment.

I also thank my husband, Mike, and my son, Jack, for their patience and support.

THIS PAGE INTENTIONALLY LEFT BLANK

I. INTRODUCTION

This investigation was conducted as part of the Office of Naval Research program for fundamental research into pulse detonation engines (PDEs). The Navy has interests in the development of a supersonic cruise missile for both time critical strike scenarios and supersonic drone targets. While pulse detonation engine technology is immature when compared to gas turbines and ramjets, the potential benefits over conventional air-breathing engines include increased thermodynamic efficiency [1], simplicity of design, and the capability to transition from subsonic to supersonic speeds without using a booster.

The fundamental differences between a detonation combustion event and the more common constant pressure combustion process, also known as deflagration, have made the implementation of pulse detonations for practical military and aviation use an attractive alternative concept for energy conversion. In a deflagration, the reaction zone, or flame front, moves at tens of meters per second, with little or no pressure change across the flame front. In a detonation, a supersonic shock wave travels at thousands of meters per second, compressing and igniting fuel and air almost instantaneously in a narrow, high-pressure heat-release zone, which is often approximated as constant volume [2].

The operational principle of a PDE is based on the repeated conversion of the chemical energy of a combustible fuel-oxidizer mixture by means of a propagating detonation. As detonation waves propagate through the mixture, large intermittent chamber pressures and corresponding thrusts are produced. Practical application of pulse detonation engines would require the use of fuels that are currently accepted by the military, including Jet-A, JP-5, and JP-10. For safety reasons, these fuels are inherently difficult to detonate with air, which adds complexity to the problem of PDE design. One way to mitigate this problem is to design a PDE with an initiator section, followed by a main combustor. The initiator is filled with a highly detonable mixture such as fuel-oxygen and is used to initiate a strong detonation wave, which then transitions into a larger main combustion section that is filled with a less-reactive fuel-air mixture.

Various initiator concepts have been investigated at the Naval Postgraduate School's Rocket Propulsion and Combustion Laboratory and are shown in Figure 1.

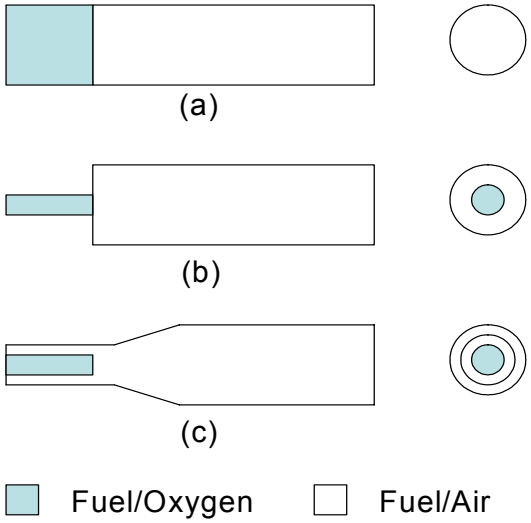

Figure 1 Initiator Concepts from Ref. [3]

Concept (a) involves the use of an oxygen-fuel "plug" at the head-end of a constant cross-sectional area combustor. Concepts (b) and (c) involve the use of a smaller cross-section initiator containing a fuel-oxygen mixture that transmits a detonation wave into a larger combustor containing a fuel-air mixture. In (b) the diffraction plane is a solid wall, while (c) allows the detonation wave to diffract to a larger diameter, but with less confinement than (b) [3]. All of these concepts involve filling the initiator with a fuel-oxygen mixture or a mixture of fuel and oxygen-enriched air. While initiating a detonation wave with these mixtures is easily achieved and reliable, the requirement of carrying auxiliary oxygen carries a penalty to performance parameters such as specific impulse and specific fuel consumption. Minimizing and/or eliminating the auxiliary oxygen requirement is critical to the future development and utilization of PDEs. Consequently, an area of concern in PDE research is the transition of detonation waves from an initiator to a larger main combustor. The current geometry of the pulse detonation engine at NPS is a valveless design, which allows for rapid filling, detonation, and purging of the combustion chamber utilizing a diffraction condition similar to geometry (c) described above. In this design, the effect of diffraction ratio on

the transmissivity of detonation waves is a key area of concern in the optimization of such an engine.

This study used a single shot detonation facility to investigate the effects of reducing the amount of auxiliary oxygen used in the initiator and the effects of increasing the expansion area ratio between the initiator and main combustor, on the successful initiation and transition of a detonation wave. The conclusions of this research can be applied to the Naval Postgraduate School's pulse detonation engine geometry to improve its cycle-to-cycle operation and overall performance.

A. DETONATION THEORY

Zel'dovich, von Neumann, and Doring developed a one-dimensional model of detonation wave structure, shown in Figure 2. They postulated that a detonation wave consisted of a shock wave moving at detonation velocity, with chemical reactions occurring behind the shock in a region much thicker than that of a typical shock wave. Figure 2 describes the change in temperature, pressure, and density across a detonation wave. First, a sudden rise occurs across the shock wave. Next, a relatively flat region occurs immediately behind the wave front, called the induction zone. Lastly, the gas properties change sharply as the reaction rate increases drastically. This is called the reaction zone [4].

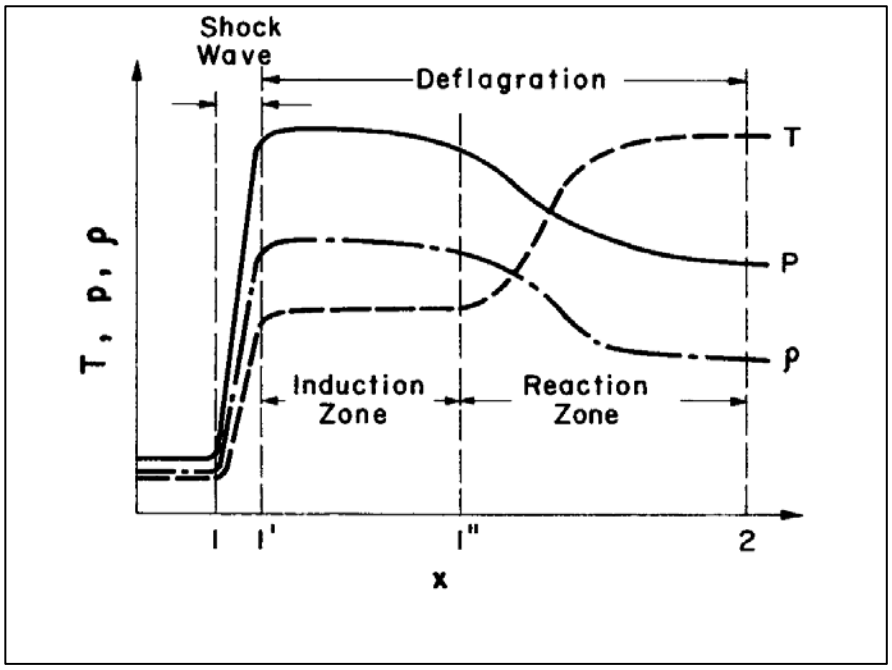

Figure 2 ZND One-Dimensional Detonation Wave Structure from Ref. [4]

In reality, the wave structure is three-dimensional and its characteristics are important to the evaluation of the wave behavior. As shown in Figure 3, transverse waves created behind the leading normal shock develop a three-dimensional cellular structure with a characteristic cell size denoted by the symbol λ. Cell size is the dimension perpendicular to the direction of propagation and is governed by the distance between the incident shock and the reflected shock [5]. As a mixture's sensitivity decreases, cell size increases. Cell size is a key parameter when attempting to detonate, diffract, and re-establish detonation waves in a particular mixture.

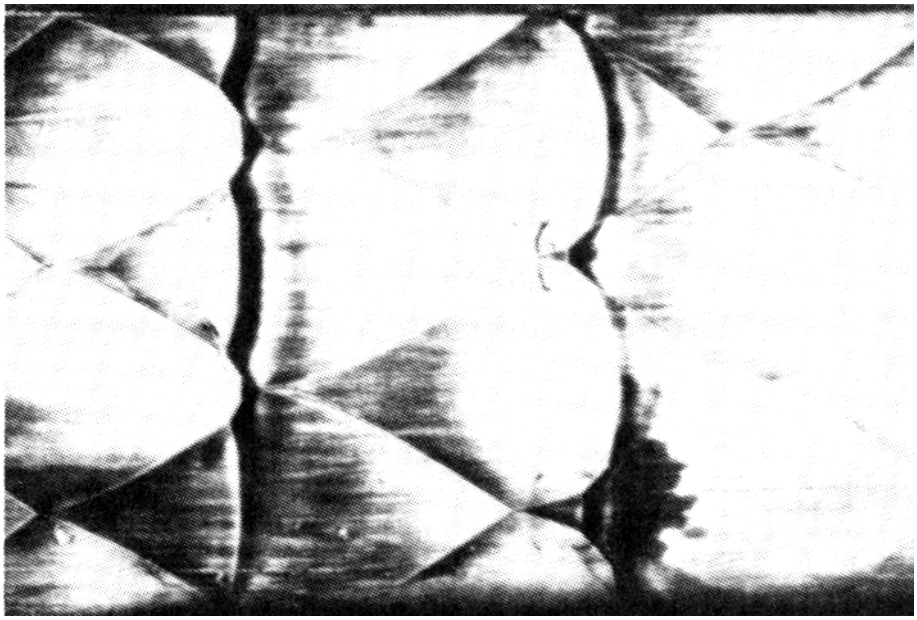

Figure 3 Smoke Foil Image of Detonation Cellular Structure from Ref. [4]

B. DETONATION DIFFRACTION

Past detonation research has developed the concept of critical tube diameter, d_c, for detonation transmission from a circular tube to an infinite volume. A detonation propagating in a tube smaller than d_c will fail when it encounters a sudden expansion into an unconfined volume of the same mixture. The critical tube diameter has been identified as 13λ, that is, 13 times the cell size of the mixture being detonated [6]. The 13λ value has been shown to be specifically valid for mixtures containing more irregular cell spacing, including fuel/air mixtures with higher activation energies. Mixtures with highly regular cell structure have been shown to often require a larger than 13λ critical diameter [7]. While the 13λ rule addresses detonation expansion in a homogeneous mixture from a small tube to an unconfined volume, a large body of recent research has focused on detonation diffraction behavior in geometries that are more analogous to that of a pulse detonation engine, namely diffraction from a small tube to a larger, finite diameter tube. Limited research exists related to the transition of a detonation wave from one mixture to another, especially when a geometric discontinuity is present.

Li and Kailasanath [6] conducted numerical simulations similar to the physical experiments in this study. In looking at the diffraction of a detonation wave from a small

tube filled with ethylene-oxygen to a larger tube filled with ethylene-air, they concluded that the strength and wave structure of the detonation in the small tube has a dominant effect on the survivability of the detonation in the large tube. Additionally, they recognized two other key factors in the wave survivability: 1) expansion waves generated at the exit of the small channel, which weaken the detonation front from its edges, and 2) the reflected shock waves from the wall that can cause reignition of the detonation wave. Teodorczyk [8] used high-speed Schlieren photography to image quasi-detonation waves, identifying auto ignition by shock reflections as the propagation mechanism for such waves in rough tubes. Oran [9], using numerical simulations, also addressed the importance of shock reflections off of a boundary and identified the reignition site directly behind the Mach stem in the lower pressure region. Murray [10, 11] looked at various diffraction geometries and the specific conditions for detonation wave reinitiation due to both spontaneous reignition and wall reflection, providing useful insight into PDE initiator design. Finally, Desbordes [12, 13] investigated overdriven detonations, in which the Mach number of the detonation wave is greater than the Mach number of a Chapman-Jouguet (C-J) detonation wave. He noted that there is a reduction in the critical diameter of the initiator tube when a detonation wave is overdriven and allowed to transition from the highly reactive mixture to the less reactive mixture, prior to diffraction. In Desbordes' studies, a membrane was inserted between the two mixtures and removed just prior to detonation. Unlike Desbordes, in this study gases were filled in sequence from the head end of the tube, with fill times calculated for each mixture based on the volume of the initiator and main combustor tubes. This setup allows for an axial spreading of the mixture gradient, which required an additional sensor to determine the length and location of the gradient.

C. PDE OPERATION

The pulse detonation engine is attractive in its simplicity of design. The simplest concept consists of a repetitive sequence of the following steps: filling a combustion chamber with reactant gases, closing one end, igniting the mixture and producing a detonation. The resulting pressures and momentum flux out of the engine vary with time but contribute to an overall thrust. The cycle begins when the tube is filled with a

combustible mixture that is subsequently ignited, resulting in the rapid transition of the deflagration wave into a detonation. This produces an elevated pressure within the combustor, which is eventually converted to a high momentum thrust. After the detonation wave exits the tube, a rarefaction wave travels back toward the head end, relieving the high pressure and removing the hot products from the combustion tube [14]. The tube is refilled and the cycle is repeated. Since this highly efficient process is inherently transient, it must be repeated many times a second to have the potential to produce large amounts of thrust. A diagram of the PDE cycle is found in Figure 4. The nearly constant volume ideal detonative cycle has been shown to be more thermodynamically efficient than a constant pressure deflagrative cycle [15], although proper conversion of thermal kinetic energy by a nozzle will be required for improved thrust generation.

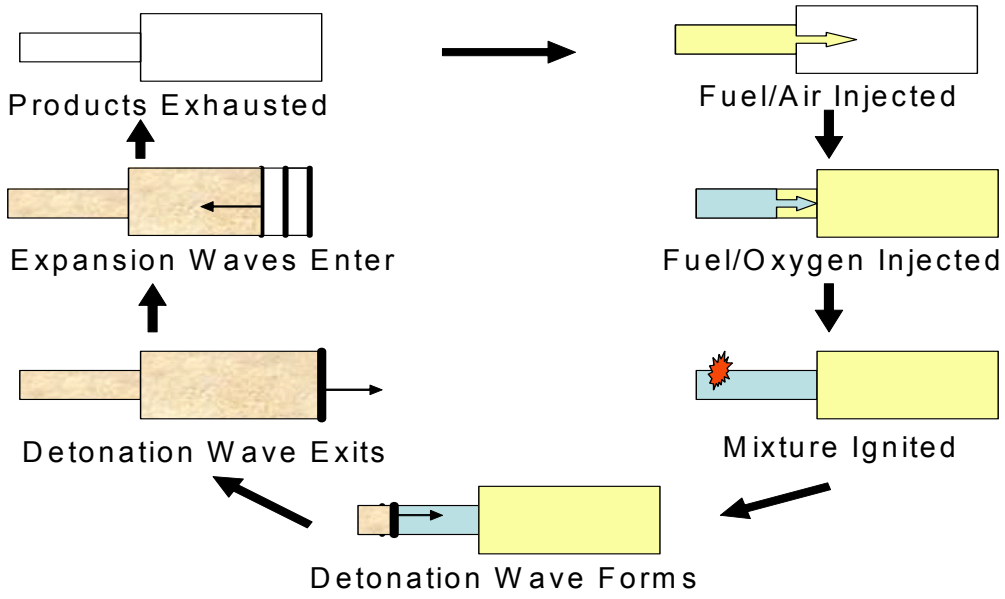

Figure 4 PDE Cycle

The ideal detonation cycle has been compared to the ideal Brayton cycle in terms of specific thrust and specific impulse. Kailasanath notes in [16], detailed simulations in which a detonation cycle with a stoichiometric hydrogen-air mixture was calculated to produce a specific thrust of 1660 N-s/kg and a fuel based I_{spf} of 5764 seconds, while calculations for the Brayton cycle yield a specific thrust of 1283 N-s/kg and an I_{sp} of

4490 seconds. Thus, at a flight Mach number of 2.1, the detonation cycle has a 28% performance gain in I_{sp} over the Brayton cycle.

The I_{sp} estimates for pulse detonation engines show great potential. However, the current design of filling the initiator tube with a fuel-oxygen mixture limits the PDE's performance. Since auxiliary oxygen is included as fuel in the specific impulse calculation, as shown in Equation (1), minimizing or eliminating the need to carry oxygen onboard is essential to the optimization of PDE design.

$$I_{SP_f} = \frac{I_T}{(m_f + m_{f\_init} + m_{O_2\_aux})g} \tag{1}$$

I_T =Total Impulse
m_f =Mass of fuel in the main combustor
m_{f_init} =Mass of fuel in the initiator
$m_{O_2\_aux}$ =Mass of auxiliary oxygen in the initiator

Since pulse detonation engines produce thrust at static conditions, their implementation in a missile system could eliminate the need for an integral booster rocket, as required with a ramjet. Although, if a particular mission requires supersonic cruise capability, then an integral rocket booster may be appropriate. Additionally, PDEs can operate over a wide range of flight Mach numbers. The projected performance parameters of PDEs show the potential for applications including guided stand-off munitions, subsonic/supersonic cruise missiles, standoff anti-air missiles, target drones, UAVs, hypersonic vehicles and combined cycle vehicles, and rocket engines [15].

While the valveless design of the Naval Postgraduate School's PDE, shown in Figure 5, provides the capability of operating at rates up to 100 Hz, it also introduces difficulty to the initiation process due to the lowered confinement conditions, requiring the use of an initiator device/section. A critical area of research in the optimization of this design is to characterize the effects of the diffraction condition between the initiator and the main combustor, specifically diameter ratio, D/D_i, where D is the main

combustor diameter and D_i is the initiator diameter at the diffraction plate, or initiator exit [3].

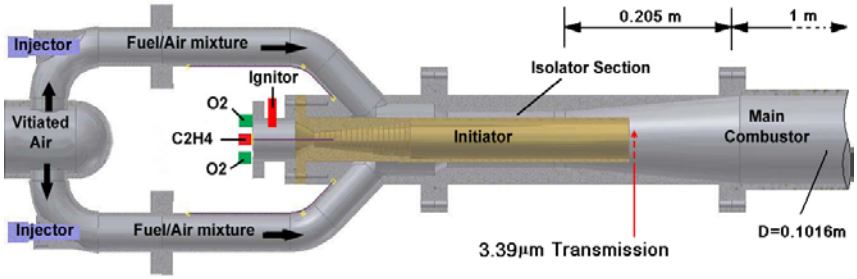

Figure 5 Diagram of the NPS Pulse Detonation Engine from Ref. [7]

Previous work at the Naval Postgraduate School has included examination of the effects of diffraction ratio on the successful propagation of detonation waves, but these were tests of detonation transition from fuel/oxygen to fuel/air mixtures. This study couples two aspects of pulse detonation engine design, optimization of diffraction ratio while minimizing the use of auxiliary oxygen in the initiator.

D. EQUIVALENCE RATIO

The term equivalence ratio is used frequently in describing the composition of the mixture used to initiate detonation events in a PDE. Equivalence ratio ϕ is defined as the molar ratio of fuel to oxidizer, divided by the molar ratio of fuel to oxidizer in a stoichiometric mixture, as shown in Equation (2).

$$\phi = \frac{\dfrac{fuel}{oxidizer}}{\left.\dfrac{fuel}{oxidizer}\right|_{stoichiometric}} \tag{2}$$

A stoichiometric mixture is one in which all reactants are used to complete the chemical reaction. In this study, ethylene, C_2H_4, was used as the fuel, therefore a stoichiometric fuel-oxygen mixture, is described by Equation (3).

$$C_2H_4 + 3O_2 \rightarrow 2CO_2 + 2H_2O \tag{3}$$

This equation shows that in this case, the stoichiometric fuel to oxidizer ratio is 1/3.

E. DETONATION WAVE IMAGING TECHNIQUES

Two imaging techniques were used to observe the characteristics of the detonation waves in this study, Shadowgraph and CH* imagery.

1. Shadowgraph Imagery

A Shadowgraph image is the second spatial derivative, or Laplacian, of the index of refraction. When compared to Schlieren imagery, which reveals the first derivative of the index of refraction, the Shadowgraph method is preferred in gas flows involving shock waves or turbulence. Shock waves produce large derivatives of refractive index that cause them to stand out as stark lines in a shadowgram [17]. The pressure discontinuity, inherent to strong shock waves is readily apparent in shadowgraph imagery.

2. CH* Imagery

When hydrocarbon fuels react with an oxidizer, the CH* radical is an intermediate by-product of the chemical reaction between ethylene, C_2H_4, and O_2. The * indicates a thermally excited state. Images depict the CH* emissions from heat release regions behind the incident shock wave and are a good marker of the beginning of the combustion process in hydrocarbon fuels. CH* is emitted between wavelengths of 428 and 431.5 nm. A filter was used on the camera to only detect the light in those wavelengths.

II. EXPERIMENTAL SETUP

All experiments for this study were conducted in the Naval Postgraduate School's Rocket Propulsion and Combustion Laboratory, Test Cell #1. Two types of single-shot detonation tubes were used, each consisting of an initiator section and a main combustor section. The first setup was an axisymmetric design; the second was a two-dimensional design with an optical section used to image detonation waves. The standard operating procedure for test cell # 1 is found in Appendix A.

A. AXISYMMETRIC TEST CONFIGURATION

The initial axisymmetric configuration consisted of an initiator section with an inner diameter of 2 inches and a length of 36 inches, followed by the main combustor with an inner diameter of 4 inches and a length of 32 inches. The gas delivery system was designed such that mixtures of ethylene, oxygen, and air were delivered into the combustor through the head end of the initiator section. Five Kistler pressure transducers were positioned along the combustors in the following locations: one transducer at the head end of the initiator (P_1), two transducers along the initiator (P_2 and P_3), 9 and 3 inches upstream of the diffraction plane, and two transducers along the main combustor (P_4 and P_5), which were 6 and 3 inches upstream of the exit, respectively. Additionally a 3.39 μm HeNe laser transmission measurement, located 3 inches upstream of the diffraction plane, was used to detect the fuel-air to fuel-oxygen gradient. A diagram of the detonation tube is found in Figure 6.

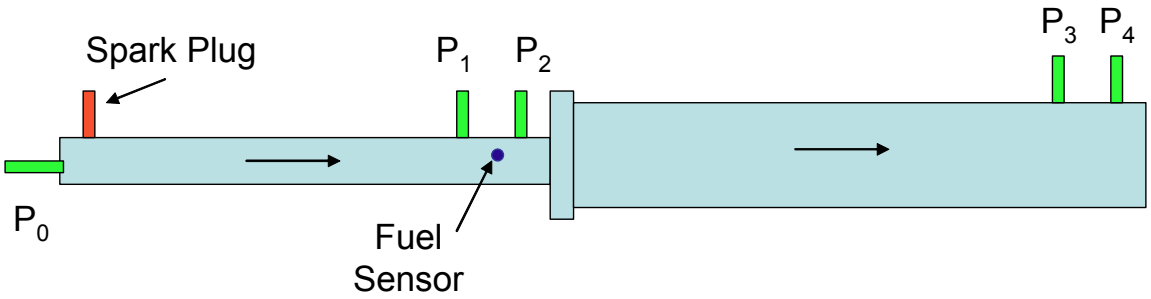

Figure 6 Axisymmetric Detonation Tube

Delivery of the gases was controlled by a ball valve and a solenoid valve for each gas, and a Visual Basic graphic user interface program remotely controlled the sequence of events for each test and the opening and closing of the valves.

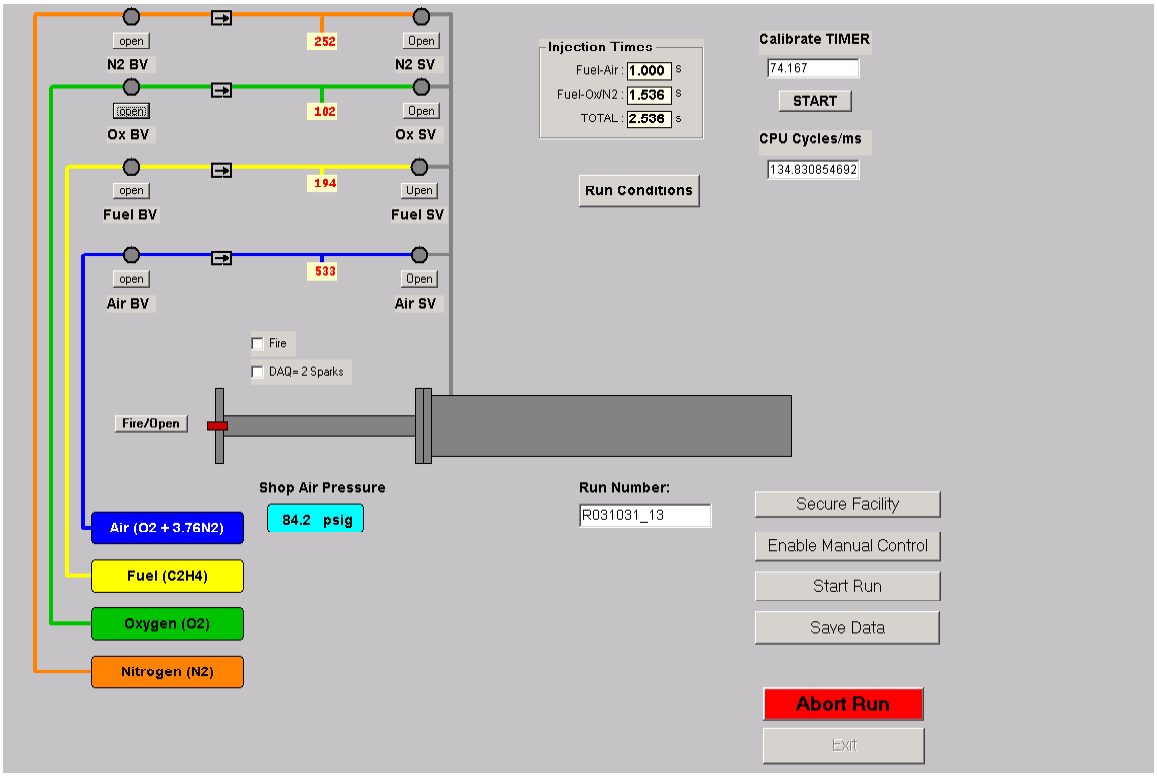

Figure 7 *Visual Basic* Facility Operations Screen

1. Equivalence Ratio Tests

The initial series of testing was conducted to find the minimum and maximum fuel-oxygen equivalence ratios that could sustain a detonation wave across the diffraction plane for the axisymmetric geometry. The Visual Basic program allowed the user to input a desired equivalence ratio, and based on a user defined fuel pressure, the required oxygen and air pressures and flow times were computed. First, the combustor was filled with a fuel-air mixture sufficient to fill the large tube. A fuel-oxygen mixture was then injected for a computed period of time to allow the mixture interface to exist across the diffraction plane. A spark discharge was introduced, 4 inches downstream of the initiator head end to initiate a detonation wave. The strength and velocity of the detonation wave was measured by the 5 pressure transducers, which output a voltage that corresponds to local static pressure at a ratio of 1 Volt to 100 psig. The outputs were recorded by a

National Instruments Lab View Data Logger and depicted graphically on the Data Logger computer.

The existence of a detonation wave was determined by the "time of flight" of the leading pressure edge or, von Neumann spike, between two transducers. By measuring wave speed in the initiator and the main combustor, it was determined whether a detonation occurred in the initiator and whether it successfully diffracted into the main combustor. In the first set of tests, the initiator equivalence ratio was incrementally increased above 1.0 then decreased below 1.0 to determine the upper and lower limits for successful detonation. The fuel-air equivalence ratio in the main combustor was held constant at 1.0.

The data logger was also used to record the fuel sensor output as well. The fuel sensor was used to observe the transition from the fuel/air mixture to the initiator fuel/oxygen/nitrogen mixture. The desire was to have as abrupt a transition as possible at the diffraction plane to provide a highly overdriven detonation wave prior to diffraction. Output showed that the transition took an average of 0.4 sec, typically resulting in an axial distance of 12 inches. Configuration modifications were made to shorten the transition distance. A cone shaped section and a flow straightener section, as shown in Figure 8, were designed and installed at the head end of the initiator tube.

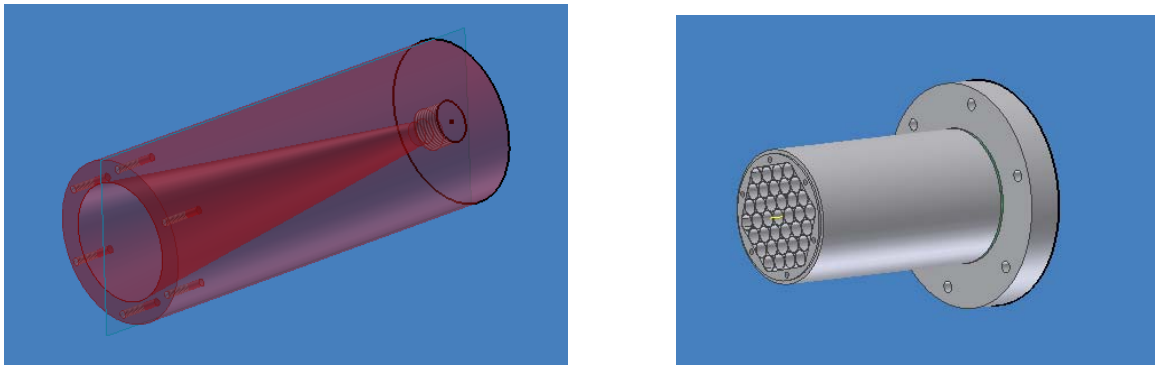

Figure 8 Cone and Flow Straightener Designs

Engineering drawings of these components are found in Appendix B. The gases were re-routed to enter at the head end of the cone section. Due to improvements in gas mixture transition, these components were used in all subsequent axisymmetric testing.

Additionally, another pressure transducer (P_4) was placed at the head end of the large tube to receive an accurate head wall pressure reading at the diffraction plane.

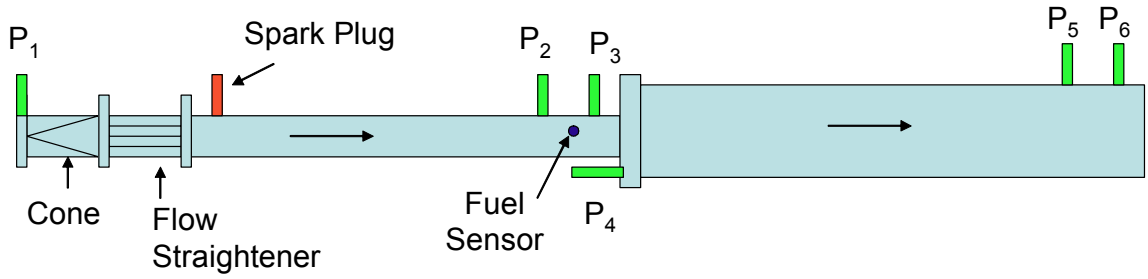

Figure 9 Modified Axisymmetric Detonation Tube

2. Nitrogen Dilution Tests

In the second set of axisymmetric tests, the fuel-oxygen mixture in the initiator section was incrementally diluted with nitrogen to determine the maximum amount of nitrogen that could be added before a detonation failed to initiate. The purpose of the testing was to find out how close to air the initiator oxidizer mixture could be and still succeed in transmitting a detonation. While the benefit of reducing auxiliary oxygen is easily calculated in the reduction of fuel mass fraction, the improvement in specific impulse must be found experimentally, due to the difficulty in determining thrust computationally. To accommodate this set of tests, nitrogen lines and valves were added to the gas delivery system and the Visual Basic program was modified to include nitrogen addition. The program was written such that one could input a desired nitrogen percentage, relative to oxygen, and the required nitrogen pressure was provided as output. These tests were conducted for equivalence ratios of 1.0, 1.5, 2.0 and 2.4. For each equivalence ratio, nitrogen was added in 5% increments until the mixture failed to detonate.

B. TWO-DIMENSIONAL TEST CONFIGURATION

The two-dimensional test configuration consisted of a series of five sections, including an optical section used to image the detonation wave. Gases were injected through four ports at the head end of a 33-inch long circular initiator tube with an inner diameter of 4 inches, followed by a 48-inch long square tube with inner dimensions of

4.5 inches per side. These first two tubes were used to initiate a strong and repeatable detonation wave prior to entering the transition section. The transition section served as the "initiator tube" if compared to the experimental setup of the axisymmetric tube. The transition section was a 14.5-inch long rectangular shaped tube measuring 4.5 inches across and a maximum vertical inner dimension of 4 inches. Plates could be added to the upper and lower sides of the tube to decrease the tube's cross-sectional area symmetrically. The transition section was followed by the 11.5-inch long optical section, which measured 4 inches in height and 4.5 inches in width. The windows were 9 inches by 3.5 inches and 1.20 inches thick. The two-dimensional test section was designed by LT Michael Fludovich for a previous effort. The details of the design and engineering drawings are found in reference [18].

1. Design Modifications

For the purposes of this study, the following modifications were made to the original design. Engineering drawings of all two-dimensional design modifications are found in Appendix B.

a. Optical Section Modifications

In the original design, the optical section expanded at a 5-degree angle along the length of the tube. For this study, a constant cross-sectional area was desired. Two 5-degree wedges were designed to modify the optical section. Reference [14] describes the injector plates used in previous experiments. Fuel was not injected through the plates in this study; rather a new set of plates was designed with holes through which the 5-degree wedges were attached. Additionally, in previous experiments the upper injector plate frame experienced structural failures at welded joints due to a detonation wave that traveled up into the void area. Brackets were designed to strengthen these joints, to avoid failures during this study.

b. Transition Section Modifications

To accommodate various area ratios in this study's experiments, 0.25-inch and 0.5 inch plates were designed to insert in the upper and lower walls of the transition

section. One set of plates with threaded holes was used as the inner most plate. The other plates were intermediate inserts with through holes.

c. Tube Extension

The fifth tube in the test section was an extension added down stream of the optical section. Pressure transducers installed in this tube allowed for detonation wave speed measurements to determine whether a detonation successfully transmitted through the optical section. The tube extension was 24 inches long with internal cross sectional dimensions of 4.5 inches x 4.5 inches. A photograph of the two-dimensional configuration is found in Figure 10. Figure 11 is a photograph taken from the downstream end of the optical section, looking toward the transition section in which three 0.5-inch plates were inserted to the top and bottom of the transition section, leaving a 1-inch channel for a 4.0 diffraction ratio.

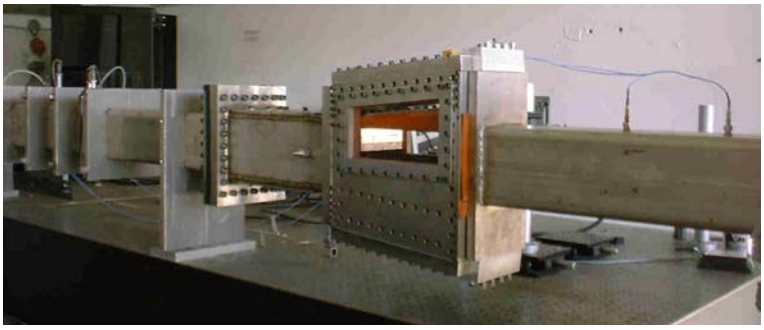

Figure 10 Two-Dimensional Test Section Photograph

Figure 11 Transition Section with Plate Inserted for a 4.0 Diffraction Ratio

A schematic diagram of the two-dimensional test section is found in Figure 12. Two pressure transducers were placed in the transition section, 6.5 and 2.5 inches upstream of the optical section, to determine wave speed prior to the diffraction plane. The pressure transducers in the tube extension were placed x and y inches down stream of the optical section. Additionally, a 3.39 μm infrared HeNe laser, used to detect the fuel-air to fuel-oxygen gradient, was positioned in the transition section, 3.5 inches upstream of the diffraction plane.

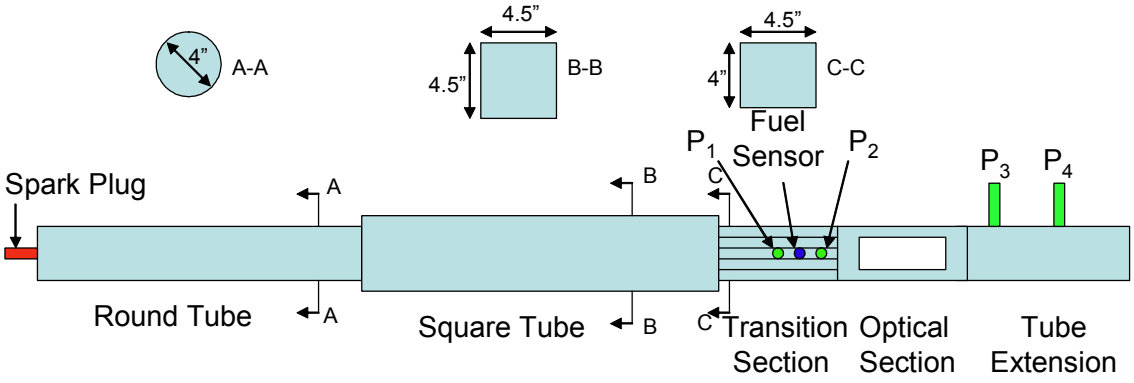

Figure 12 Two-Dimensional Test Section Diagram

2. CH* Imagery

A Princeton Instruments (Roper Scientific) intensified CCD camera was used to take CH* chemiluminescence images of the detonation wave. A narrow band interference filter centered at 430 nm, with a filter Full Width Half Maximum (FWHM) of 10nm (CVI Laser Corporation: Part # F10-430.0-4-2.0) was installed. The camera used Winview 32 software to output one image per test with a 16-bit color scale that represents increasing emission. The triggering of the intensifier occurred when pressure transducer, P_2, read at least 2 Volts, indicating the time of arrival of the detonation wave. To receive a sequence of images as a wave travels through the optical section, a series of tests are conducted with increasing camera delay.

3. Shadowgraph Imagery

The Princeton Instruments camera setup was modified to take Shadowgraph images of the detonation waves. In this configuration, a Spectra-Physics Stabilite 2017-

05 Argon-Ion 7 Watt laser, with primary wavelengths at 488 nm and 514.5 nm was used. The light was directed through a spatial filter to appear as a point source. A series of mirrors, as shown in Figure 13, directed the light through the optical test section and onto the imaging camera. As with the CH* imagery, timing of the shadowgraph camera was based on trigger pulse sent by the pressure transducer upstream of the optical section, transducer P_2 and the camera time delay was adjusted to obtain a series of images at various points within the field of view.

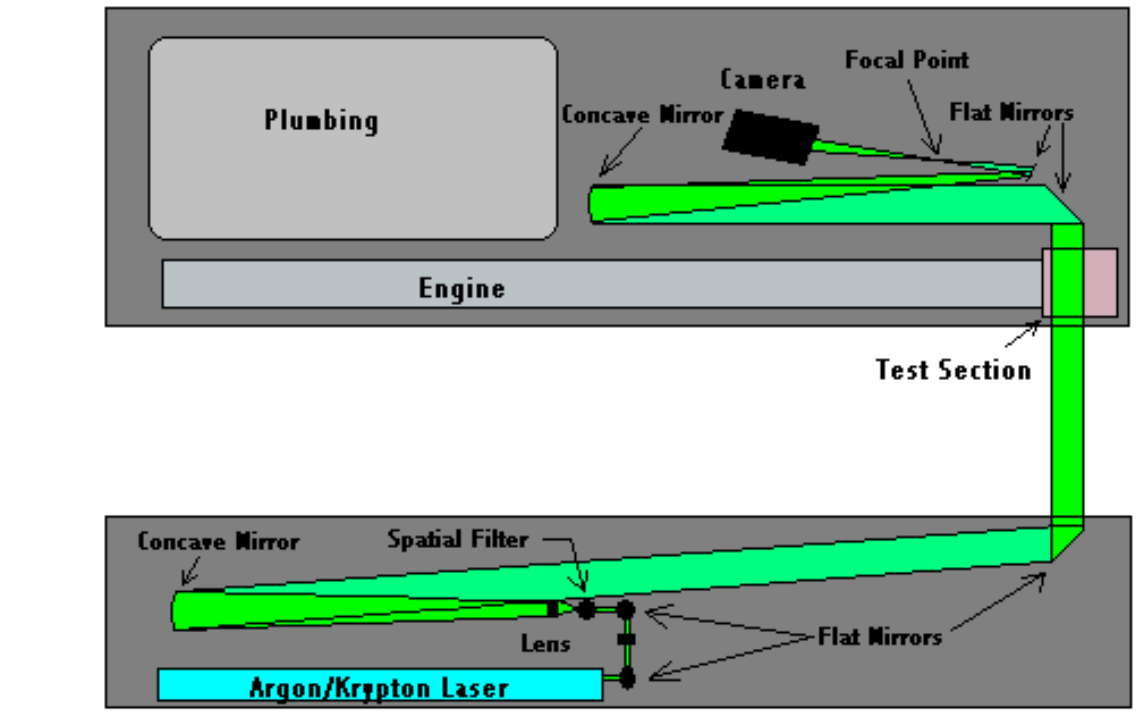

Figure 13 Shadowgraph Set-up from Ref. [18]

III. RESULTS

A. AXISYMMETRIC TEST CONFIGURATION

1. Wave Speed Calculations

A fuel-air combustion wave is determined to be a successful detonation when its wave speed is greater than or equal to 1.5 km/s, which corresponds to about Mach 5, relative to the unburned reactants. The wave speed in the initiator was measured by the distance between pressure transducers P_2 and P_3 divided by time difference of the detonation wave arrival at those transducers. Pressure transducers P5 and P6 measured the wave speed in the main combustor. In phase 1 of the axisymmetric testing, where the initiator section was filled with a fuel-oxygen mixture and the main combustor section was filled with a fuel-air mixture, successful detonations were observed for equivalence ratios ranging from 0.8 to 3.0. A table of the phase 1 test results is found in Appendix C.

In phase 2, nitrogen dilution tests were conducted for equivalence ratios of $\phi = 1.0, 1.5, 2.0, 2.4$. The detonation velocities versus nitrogen concentration in the initiator mixture were plotted for each equivalence ratio tested. As shown in Figure 14, approximately half of the detonations in the initiator section failed when nitrogen content was 45% and 50%. When nitrogen content was increased to 55%, all detonations failed to initiate. As shown in Figure 15 approximately half of the detonations in the main combustor failed when nitrogen content was 55 and 60 %. When nitrogen content was increased to 65%, all detonations failed. The results show that while a detonation may have failed to initiate in the initiator tube with nitrogen contents as low as 45%, through constructive interference such as wall reflections and shock-shock interactions, a detonation wave initiated in the main combustor for up to 60% nitrogen dilution.

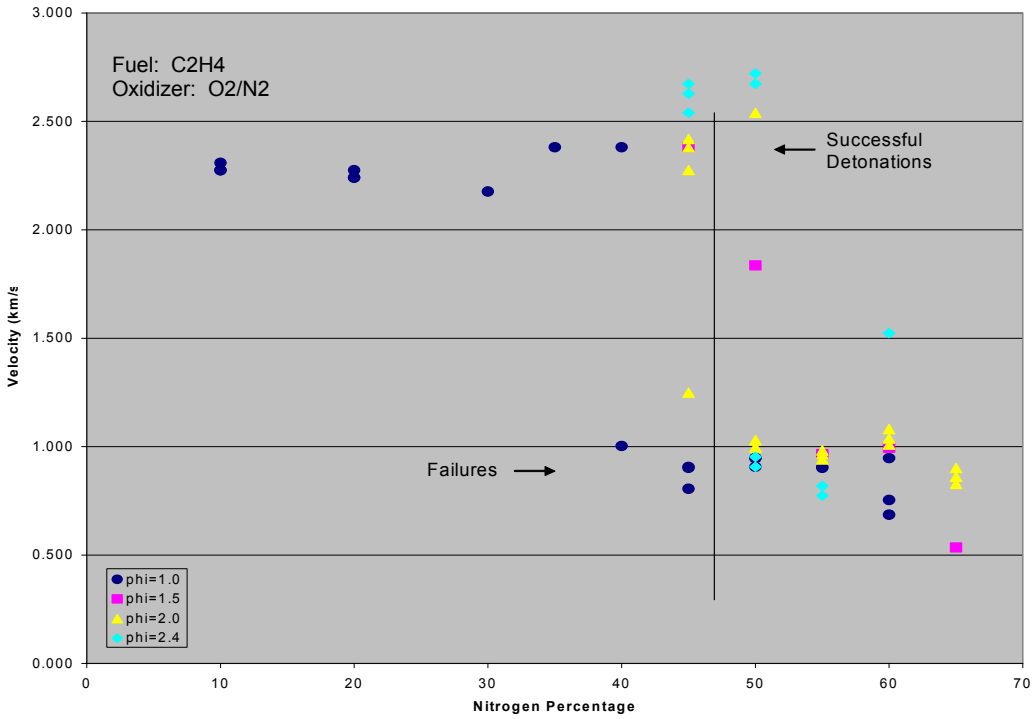

Figure 14 Detonation Velocity in the Initiator vs. Nitrogen Concentration in the Initiator Mixture

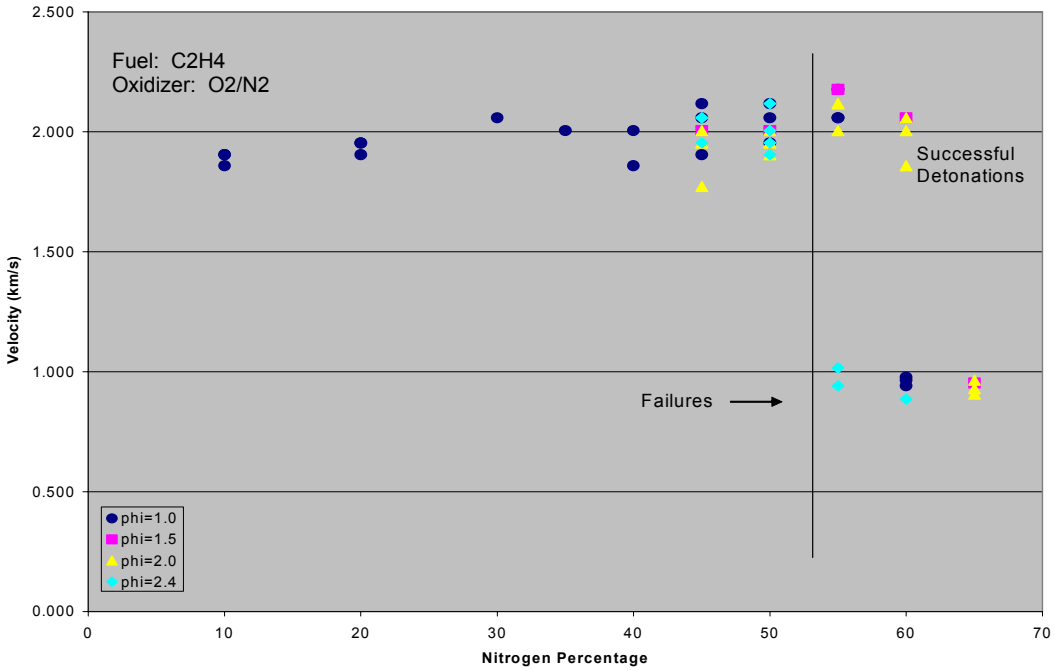

Figure 15 Detonation Velocity in the Main Combustor vs. Nitrogen Concentration in the Initiator Mixture

2. I_{sp} Calculations

A Matlab program was written to calculate specific impulse (I_{sp}) of each test case using the pressure data from the head ends of the initiator section and the main combustor section. The code was initially written for phase 1 of axisymmetric testing, to accommodate the equivalence ratio tests. The code was then modified to accommodate the nitrogen dilution testing conducted in phase 2. The Matlab code is found in Appendix D.

The Matlab program reads a .txt file that contains a list of the file names for each set of pressure data as well as the fuel/oxygen equivalence ratio used in the respective test. Then the Matlab program runs in a loop until it has read the data files for all test cases. The data is output as voltages from the Kistler pressure transducers through the amplifiers. The amplifiers can be set so that 1 Volt equals 100, 200, or 300 psi. The Matlab program converts the voltages to psi and then to Pascals. Then every 5 data points are averaged to reduce the possibility of misleading results from a single anomalous voltage reading. Next the maximum pressure at each transducer is assumed to be the von Neumann spike, which is the sudden pressure rise that indicates the presence of a detonation wave. Total impulse is calculated by integrating the area under the pressure plot over time, as shown in Equation (4).

$$I_t = \int PAdt \tag{4}$$

Specific impulse is calculated by dividing total impulse by the mass of the fuel. In specific impulse calculations the mass of auxiliary oxygen is considered to be part of the total fuel mass.

The Matlab program was modified for the nitrogen dilution tests to account for the volume added to the initiator section with the addition of the cone and flow straightener. Additionally the fuel mass calculation in the code was modified to account for the varying nitrogen content in the initiator mixture. Since the calculation depended upon the percentage of nitrogen, this variable was as a third column in the .txt file, along with the list of file names and equivalence ratios.

For each test case, the Matlab program plots head end pressures vs. time. An example of the output plot is found in Figure 16. P_1 is the pressure at the head end of the initiator tube. P_4 is the pressure at the head end of the main combustor. Next, the Matlab code plots total impulse vs. time; an example is shown in Figure 17. The total impulse plot includes annotation of the maximum impulse at the locations of P_1 and P_4. The user is then asked to confirm that the correct location was chosen, prior to iterating to the next case. If the chosen location is incorrect the user has the opportunity to input the correct location. Appendix C contains the tabulated data of the axisymmetric nitrogen dilution tests output from the Matlab program.

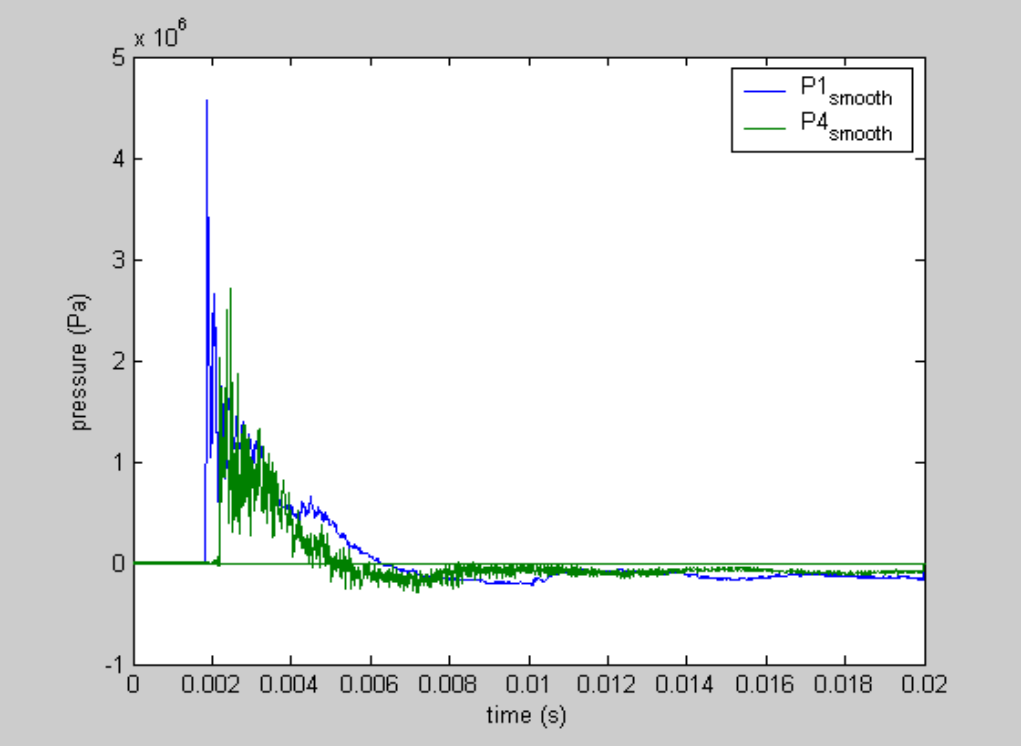

Figure 16 Sample Pressure Output

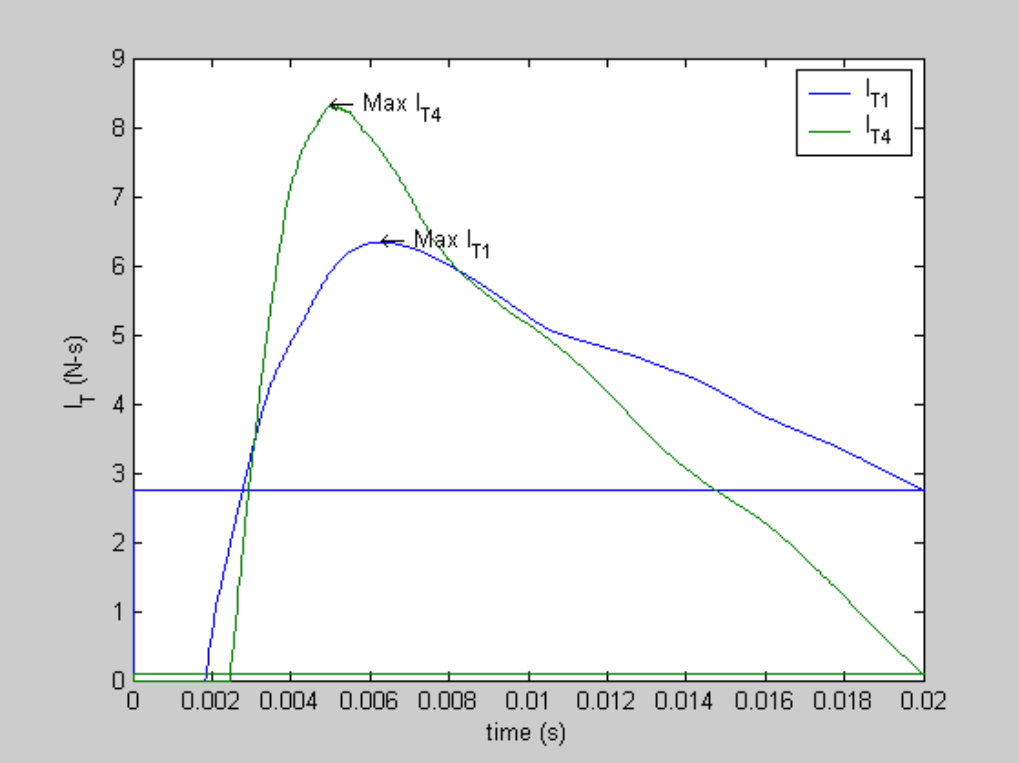

Figure 17 Sample Total Impulse Plot

Figure 18 is a plot of specific impulse (I_{sp}) vs. nitrogen concentration for various fuel rich equivalence ratios. We can see that I_{sp} increases with decreasing nitrogen content, until the nitrogen content is too high to sustain a detonation wave. The higher the equivalence ratio the lower the I_{sp}. This shows that carrying additional fuel will decrease specific impulse, as expected. The results also showed that it took lower nitrogen content to cause a failure of the mixture to detonate for an equivalence ratio of 2.4, than for the 1.5 and 2.0 equivalence ratios.

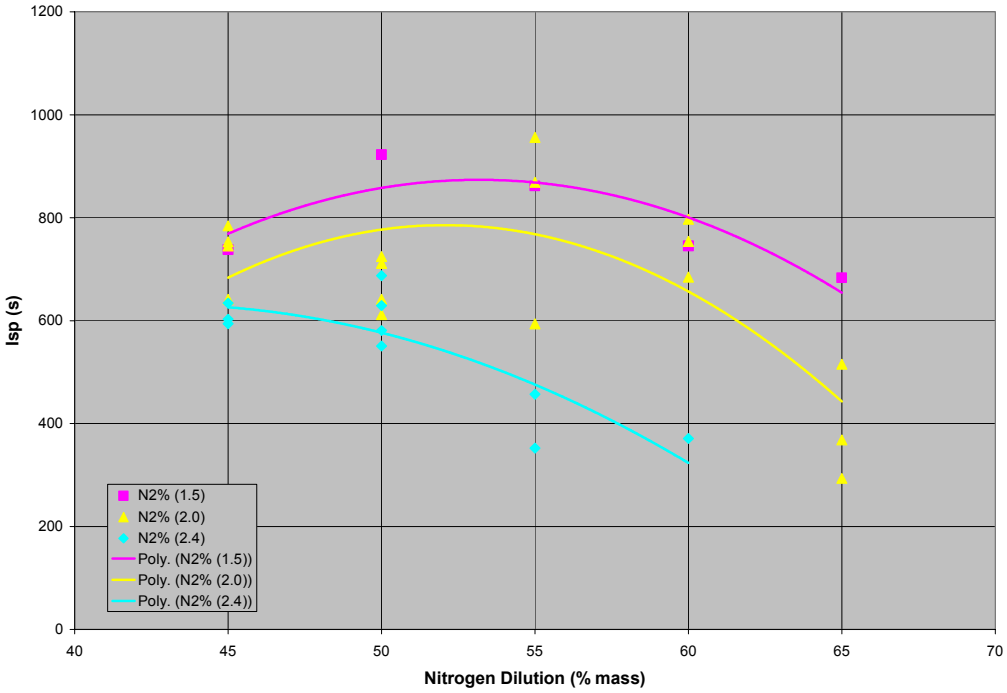

Figure 18 Isp vs. Nitrogen Dilution for Varying Equivalence Ratios

B. TWO-DIMENSIONAL TEST CONFIGURATION

1. Wave Speed Results

The results of the nitrogen dilution testing for various diffraction ratios are found in Table 1. The first column of the table, test height, refers to the vertical dimension of the transition section. Since the dimensions of the optical section remained constant, with a vertical dimension of 4 inches, the diffraction area ratio is $\frac{4}{TestHeight}$.

Test Height (in)	Area Ratio	N_2 Dilution (Success)	N_2 Dilution (Failure)
3.0	1.33	79%	N/A
2.5	1.60	79%	N/A
2.0	2.00	79%	N/A
1.5	2.67	79%	N/A
1.0	4.00	65%	70%

Table 1. Two-Dimensional Test Configuration Results

Initiator wave speed was calculated using pressure transducers in the transition section, P_1 and P_2. Wave speed in the main combustor was calculated using pressure transducers in the tube extension, P_3 and P_4. As with the axisymmetric tests, a wave speed of 1.5 km/s or greater was considered to be a detonation. For area ratios of 1.33 to 2.67, detonation waves successfully transmitted for all nitrogen dilution cases, including 79%, which is the equivalent of a fuel-air mixture in the initiator. For an area ratio of 4.0, detonation waves successfully transmitted with 65% nitrogen dilution but failed with 70% nitrogen dilution. A table of wave speed results is found in Appendix E.

2. Shadowgraph Imaging Results

The camera used in this study was capable of taking one image per detonation event. Therefore, to obtain a sequence of wave images as the detonation traveled through the optical test section, the camera delay was varied for several consecutive runs of each test case. The time, in microseconds, listed below each image is the delay between the time the camera was triggered by a passing detonation wave at pressure transducer, P_2, until the image was taken. The images referred to in the results section were all taken during the 4.0 area ratio test cases. These test cases were the focus of the imagery study due to the interest in determining the causes of detonation wave failure in the higher nitrogen dilution tests.

a. 35% Nitrogen Dilution

Figure 19 is a series of Shadowgraph images for the test case of 35% nitrogen dilution in a 4.0 area ratio. The 55 μs image shows evidence of a vertical wave front in the center of the detonation with curvature above that indicates weakening of the wave as it diffracts. In the next three images, the marbled areas behind the shock wave generally indicate the strong heat release regions in which the final stages of the chemical reaction between ethylene, C_2H_4, and O_2 take place, resulting in the production of CO_2 and H_2O. The close coupling of the heat release region to the wave front is indication of a strong detonation wave. The detonation waves in this test case successfully transmitted into the extension tube, as determined by wave speed measured by the pressure transducers.

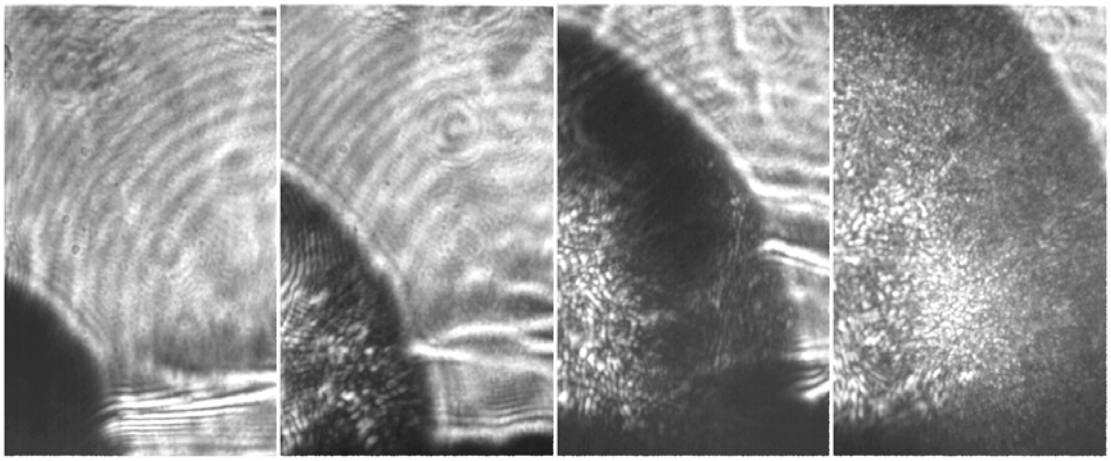

55 μs 65 μs 75 μs 80 μs

Figure 19 Shadowgraph Images with Area Ratio of 4.0 and 35% N_2 Dilution

b. 65% Nitrogen Dilution

The series of images found in Figure 20 were taken for an area ratio of 4.0 and 65% Nitrogen dilution. The first 6 frames were taken with the camera's field of view beginning at the diffraction plane. Images 7 and 8 were taken with the camera moved down stream. In these images the marbled heat release zone that has separated from the wave front as compared to the 35% nitrogen dilution case. In frames 4 through 8, newly formed shockwaves appear, which are likely due to constructive interference between the lateral waves traveling behind the detonation. The camera was moved downstream to

look for evidence of Mach stems that could be aiding in the re-initiation of the detonation wave. No evidence of this was found, although the 65% nitrogen dilution case did successfully transmit. There could be two reasons for this. First, Mach stems could be occurring downstream of the optical section, out of the camera's field of view. Second, the detonation wave may be re-initiating due to shock-shock or shock-flame interactions only.

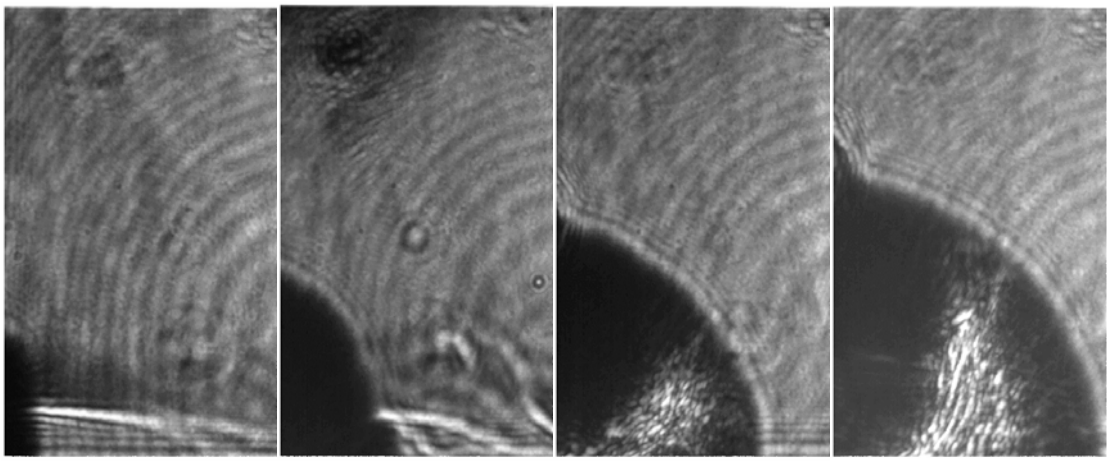

55 μs 60 μs 65 μs 70 μs

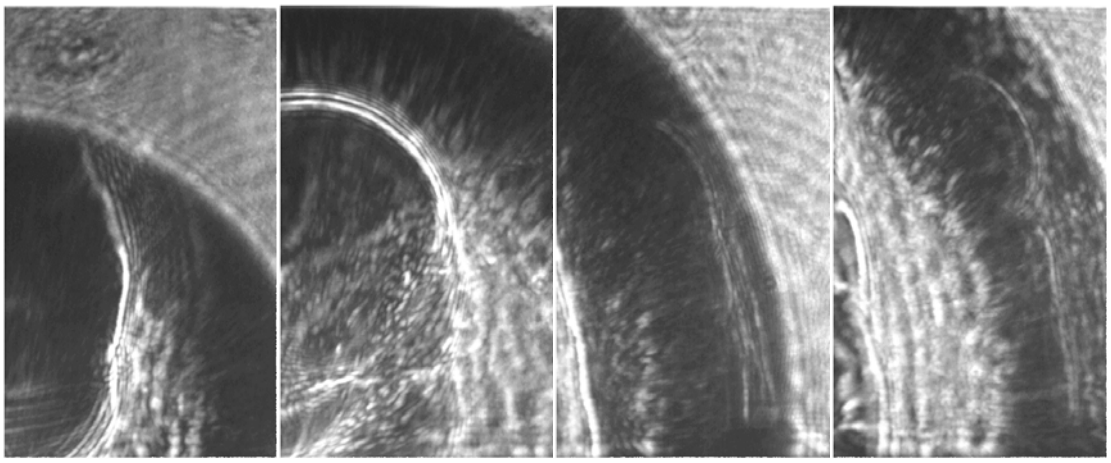

75 μs 90 μs 100 μs 110 μs

Figure 20 Shadowgraph Images with Area Ratio of 4.0 and 65% N_2 Dilution

c. 79% Nitrogen Dilution

The images taken at 79% nitrogen dilution, which is the equivalent of a fuel-air mixture in the initiator, show the failing detonation wave. In the first three frames, no marbled heat release region is evident in the field of view of the camera, leading to the conclusion that any heat release region that exists is largely decoupled from the wave front. The fourth frame shows a possible heat release region close to the wave front that appears to be a random shock-shock interaction. The 79% nitrogen dilution tests were cases in which the detonation wave failed to transmit. Any shock-shock interactions that occurred were too sporadic or non-repeatable to successfully reinitiate the detonation.

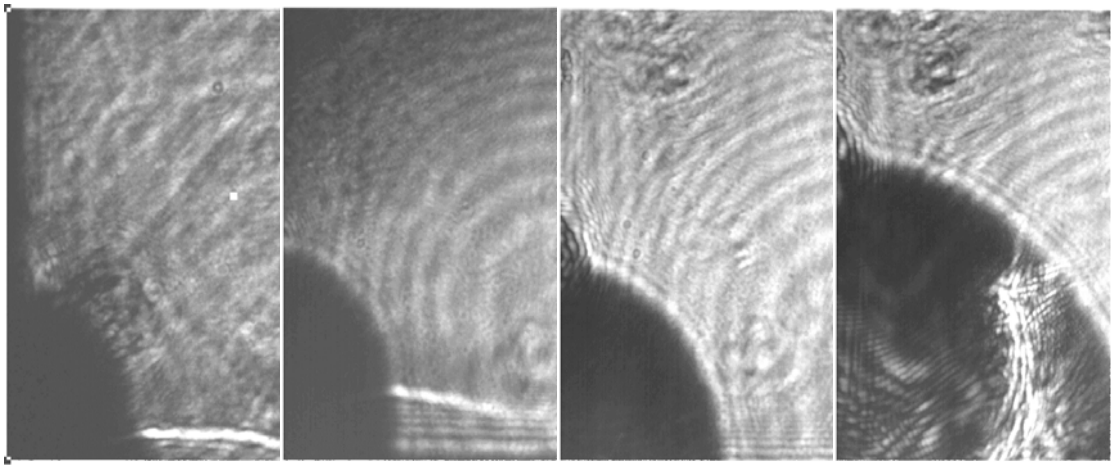

60 μs 65 μs 70 μs 80 μs

Figure 21 Shadowgraph Images with Area Ratio of 4.0 and 79% N_2 Dilution

3. CH* Imaging Results

The images discussed below are all CH* imagery, taken for various levels of nitrogen dilution at an area ratio of 4.0. CH* images taken at other area ratios are found in Appendix F.

a. 45% Nitrogen Dilution

The images found in Figure 22 were taken at 45% Nitrogen dilution, while the detonations were successfully transmitting. Strong CH*emissions were visible

throughout, as indicated by the pink regions. The blue regions indicate low CH* emissions.

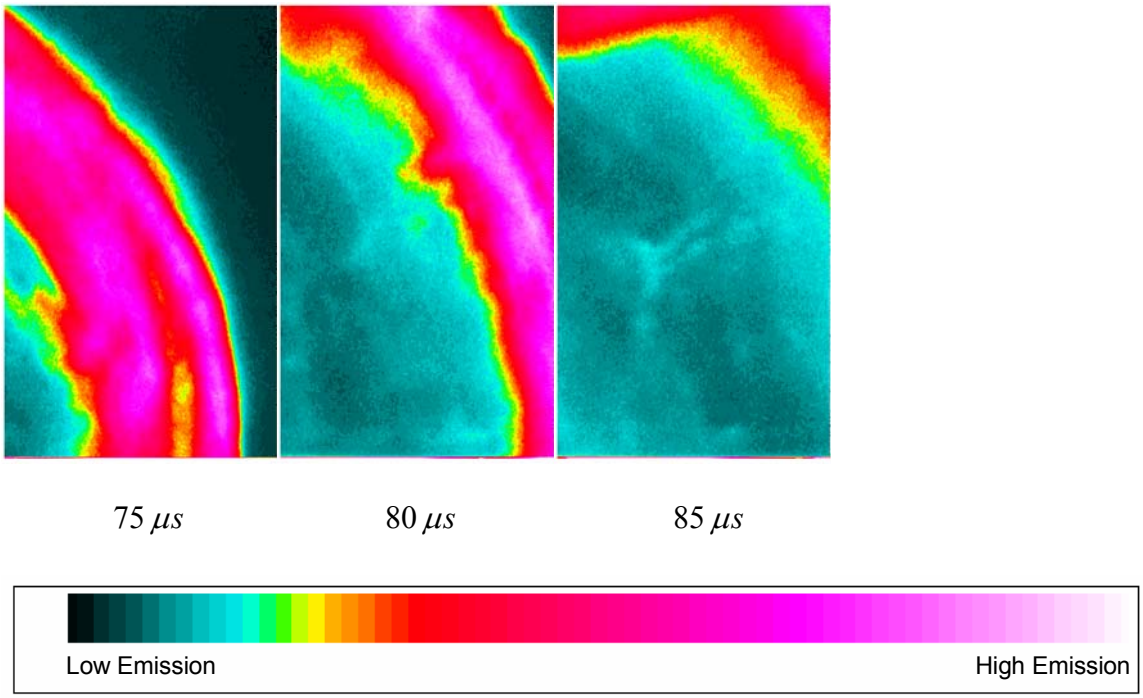

Figure 22 CH* Images with Area Ratio of 4.0 and 45% N_2 Dilution

b. 65% Nitrogen Dilution

The images taken at 65% Nitrogen dilution, found in Figure 23, show regions of strong CH* emission that diminish as time goes on. The detonations in this test case were still successful in transmitting although the regions of intense CH* emission were smaller than the 45% Nitrogen dilution case.

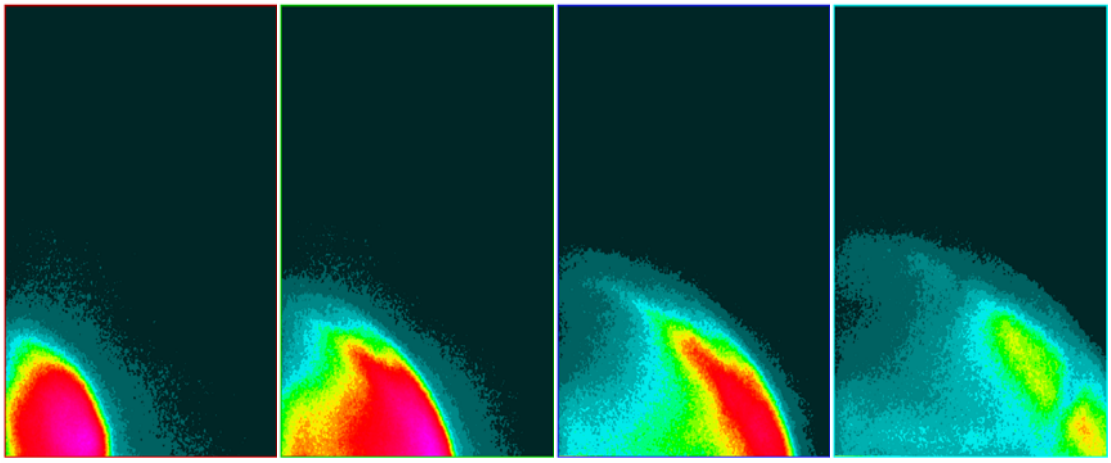

55 μs 60 μs 65 μs 70 μs

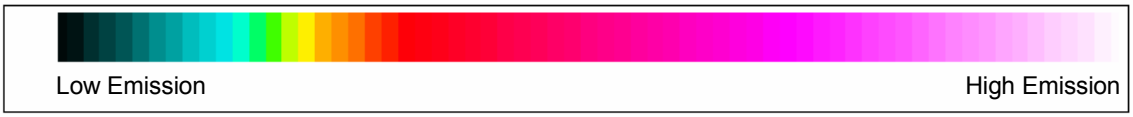

Figure 23 CH* Images with Area Ratio of 4.0 and 65% N_2 Dilution

c. 79% Nitrogen Dilution

The images taken at the 79% Nitrogen dilution case show a small region of strong CH* emission in the first frame that deteriorates to weak emission by the third frame. This was a case where the detonation wave failed to transmit.

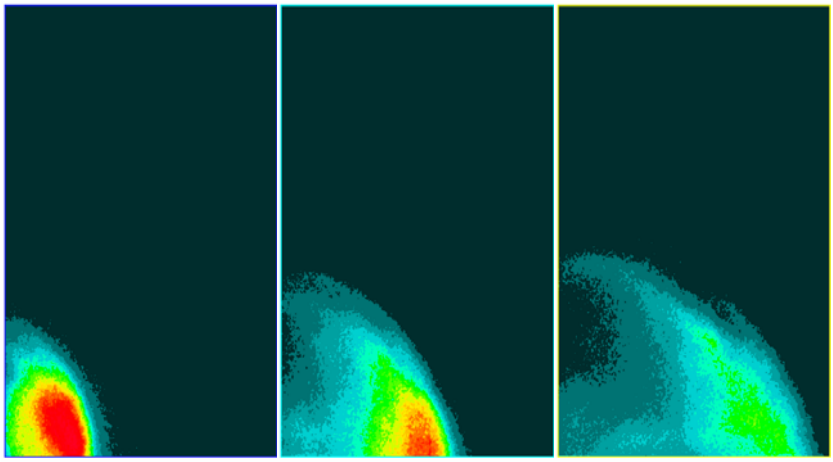

65 μs 70 μs 75 μs

Figure 24 CH* Images with Area Ratio of 4.0 and 79% N_2 Dilution

IV. CONCLUSIONS AND FUTURE WORK

Diluting a fuel-oxygen initiator mixture with increasing amounts of nitrogen weakens a detonation wave that is intended to diffract into a larger main combustor. In previous studies with pure fuel-oxygen mixtures in the initiator, the detonation re-initiation mechanism after diffraction was due to strong shock reflection with the main combustor walls, also known as a Mach stem. In this study, when the initiator mixture was weakened by nitrogen dilution to the equivalent of a fuel-air mixture (79% N_2), detonation waves succeeded in transmitting for diffraction ratios up to 2.67, although Mach stems were not evident in the CH* or Shadowgraph imagery. The re-initiation mechanism therefore appears to be via shock-shock or shock-flame interactions behind the wave front that eventually strengthened the leading shock wave enough to successfully transmit/re-initiate a detonation into the larger combustor. At a diffraction ratio of 4.0, the detonation waves successfully transmitted at 65% nitrogen dilution although the re-initiation mechanism appeared to be chaotic explosions behind the wave front. The axisymmetric test cases exhibited lower thresholds for detonation wave failure, but this is expected because of the 3-D versus 2-D expansion condition. It was concluded that the two-dimensional test configuration enabled transmission of detonation waves at higher nitrogen dilution concentrations than the axisymmetric configuration because the horizontal dimension remains constant across the diffraction plane for the two-dimensional test section and only diffracts in the vertical direction. This condition allows the detonation wave to experience less expansion at the diffraction plane than in the axisymmetric cases.

The next step to further this effort would be to implement a diffraction configuration that more closely resembles the initiator to main combustor interface of the Naval Postgraduate School's Pulse Detonation Engine. Instead of a diffraction plane that is a solid wall, the innermost transition section inserts would extend into the optical section. Upon diffraction, the detonation wave would be able to expand back into the cavity between the initiator and main combustor, upstream of the diffraction plane. The nitrogen dilution test matrix should be conducted again for this plate extension

configuration to determine the limits for successful detonation wave transmission for fuel-air mixtures as well as for other fuel-oxidizer combinations.

APPENDIX A. CELL #1 STANDARD OPERATING PROCEDURE

1. Call the golf course to notify golfers of testing (x2167).

2. Ensure Emergency Shutdown is depressed.

3. Turn on AC/DC Power Supply.

4. Turn on yellow lights. (required when gases are pressurized).

5. Turn on laser light.

6. Connect laser fiber optic cable to detonation tube.

7. Turn laser on. Warm up 30 minutes.

8. Turn on Tripp Lite surge suppressor.

9. Set Kistler amplifiers to *Operate* (for pressure transducers).

10. Turn on Stanford amplifier (for fuel sensor).

11. Turn on Tescom 24V Power Supply ON (provides power to pressure regulators).

12. Open shop air valve. (provides air to ball valves)

13. For Cold Flow – Disconnect Spark Plug. For Hot Run – Ensure Spark Plug is connected.

14. Test fuel sensor:

a. Connect voltmeter (DC) to output side of pre-amplifier.

b. Adjust fiber optic cable until voltmeter reads at least 0.3 V.

c. Reconnect output.

15. Ensure pressure transducers are connected.

16. Rope off area in front of laser.

17. Procedure for turning on the Roper Scientific Camera (CH imagery).

a. Power on the ST-138 Controller for the Roper Scientific camera.

b. When first adjusting camera, ensure MCP Power is OFF, and Brightness Control is ON (found on the back of the PG-200).

c. Power on the PG-200.

d. Set cooler to -30 degrees.

e. Turn cooler on.

f. Once camera settings are adjusted, MCP Power ON, Brightness Control OFF.

g. Set desired Gate Delay and Gate Width.

h. Function 77 – changes Gain (up to 1000V).

i. On computer, Click on Winview 32.

j. Click Acquire to start.

18. Open Air supply valve (outside, on the ground).

19. Set Oxygen (Node 2), Fuel (Node 3), and Air (Node 4) pressures to 0 psi, using ER3000 software.

20. Open Oxygen, Fuel and Nitrogen tanks. Fuel must read at least 500-600 psi.

21. Reset the Emergency Shutdown.

22. Set desired Fuel pressure using ER3000 software (Node 3).

23. Close ER3000 program.

24. Open Detonation Diffraction Software:

a. Click on *Det. Diffraction* icon.

b. Click on *Enter*.

c. Click on *Facility Operations*.

d. Click on *Open Facility*.

e. Click on *Enable Manual Control*.

f. Click on *Open* Fuel ball valve.

25. Click on *Run Conditions*.

26. Set equivalence ratios, Nitrogen percentage, and Transition Tube height.

27. Click on *Calculate* for required Oxygen and Air pressures.

28. Set Oxygen (Node 2) and Air (Node 4) pressure using ER3000 Program.

29. Close ER3000 program.

30. Set Nitrogen pressure using manual regulator at the bottle.

31. Open Oxygen, Air, and Nitrogen ball valves to check line pressure.

32. Click on Secure Facility.

33. Click on Open Facility.

34. Enter Run Number.

35. Enter pressures, times, and equivalence ratios into Log book.

36. Turn on National Instruments Equipment.

37. Open *Mike's Data Logger* icon.

38. Set Scan rate.

a. Cold Flow – 10,000 Hz, 30,000 scans

b. Hot Run – 1 MHz, 10,000 scans

39. Notify people that we are about to flow gases.

40. For Hot fire only:

a. Check for golfers.

b. Turn on Siren.

c. Press Record on VCR.

41. Check *Fire, DAQ* and *Fire* for Cold Flow, Check *Fire* only for Hot Fire.

42. Click *Acq* on Winview 32.

43. Click *Run* on data logger.

44. Click *Run* on Facility Operations (within 25 seconds).

45. Save Data on data logger.

46. Save Data on Facility Operations.

47. Input results into logbook spreadsheet.

Procedure for Transition between Cold Flow and Hot Fire

1. Purge lines.

2. Click on *Secure Facility.*

3. Depress Emergency Shutdown.

4. Connect/Disconnect sparkplug.

5. Reset Emergency Shutdown.

6. Modify data logger settings.

7. Go to step 39 of previous procedure.

Shutdown Procedure

1. Set Oxygen and Fuel pressures to 0 psi, set Air pressure to 50 psi using ER3000 software.

2. Close Fuel and Oxygen and Nitrogen tanks.

3. Purge Oxygen, Fuel, and Nitrogen lines with Air flowing.

4. Close all Ball and Solenoid Valves.

5. Set Air pressure to 0 psi with ER3000 software.

6. Purge Air line.

7. Click on *Secure Facility*.

8. Click on *Exit.*

9. Depress *Emergency Shutdown.*

10. Close outside Air valve.

11. Turn camera cooler and PG-200 off.

12. Leave camera power on for 5 minutes.

13. Turn off power in cell:

a. Tescom 24V power supply to off.

b. Stanford amplifier to off.

c. Tripp Lite surge suppressor to off.

14. Turn laser off.

15. Disconnect fiber optics cable.

16. Turn camera power supply off.

17. Turn laser light off.

18. Turn AC/DC power supply off (inside).

19. Turn off yellow lights.

THIS PAGE INTENTIONALLY LEFT BLANK

APPENDIX B. ENGINEERING DRAWINGS

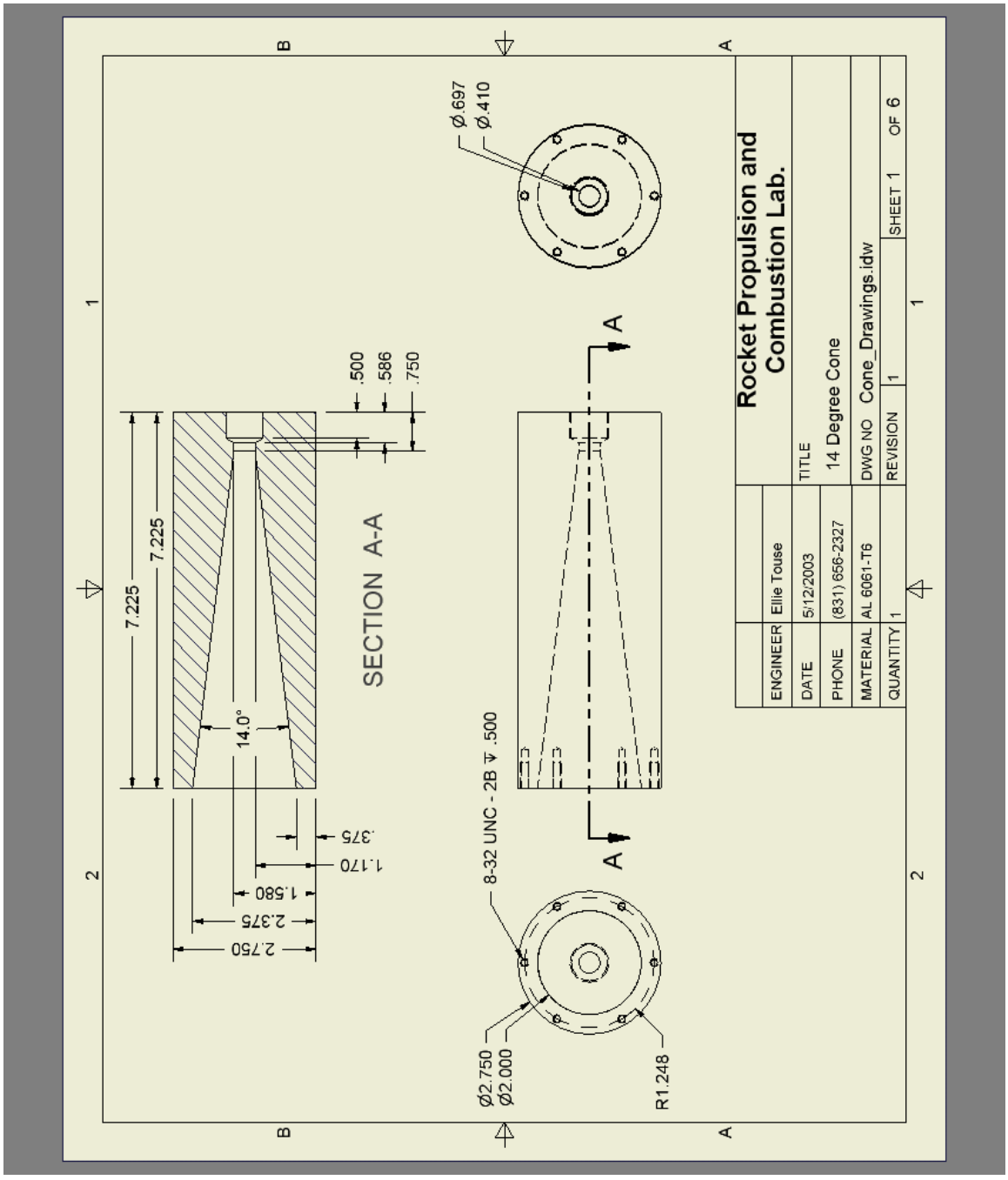

Figure 25 Cone for Axisymmetric Test Section

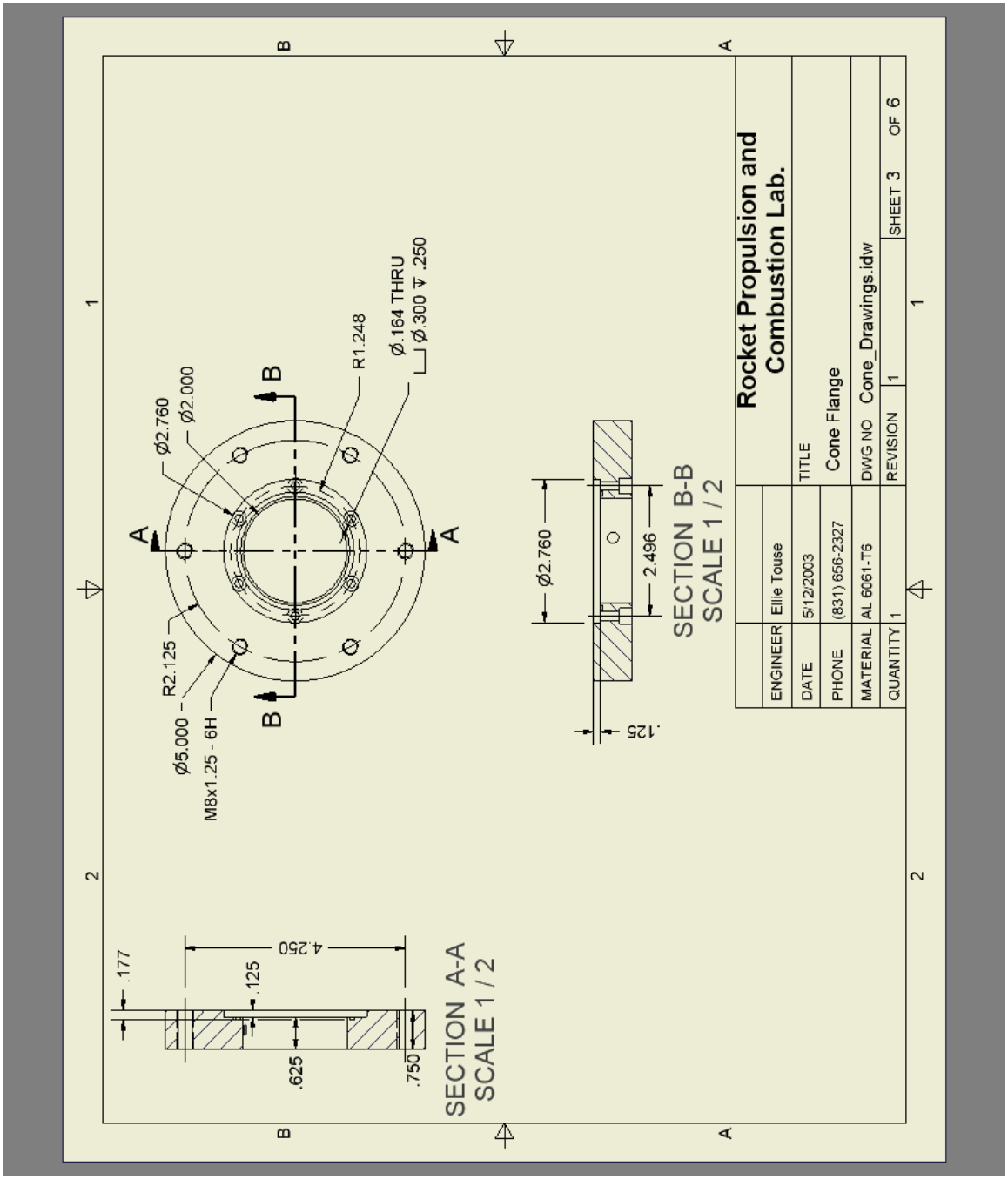

Figure 26 Cone Flange for Axisymmetric Test Section (Drawing 1 of 3)

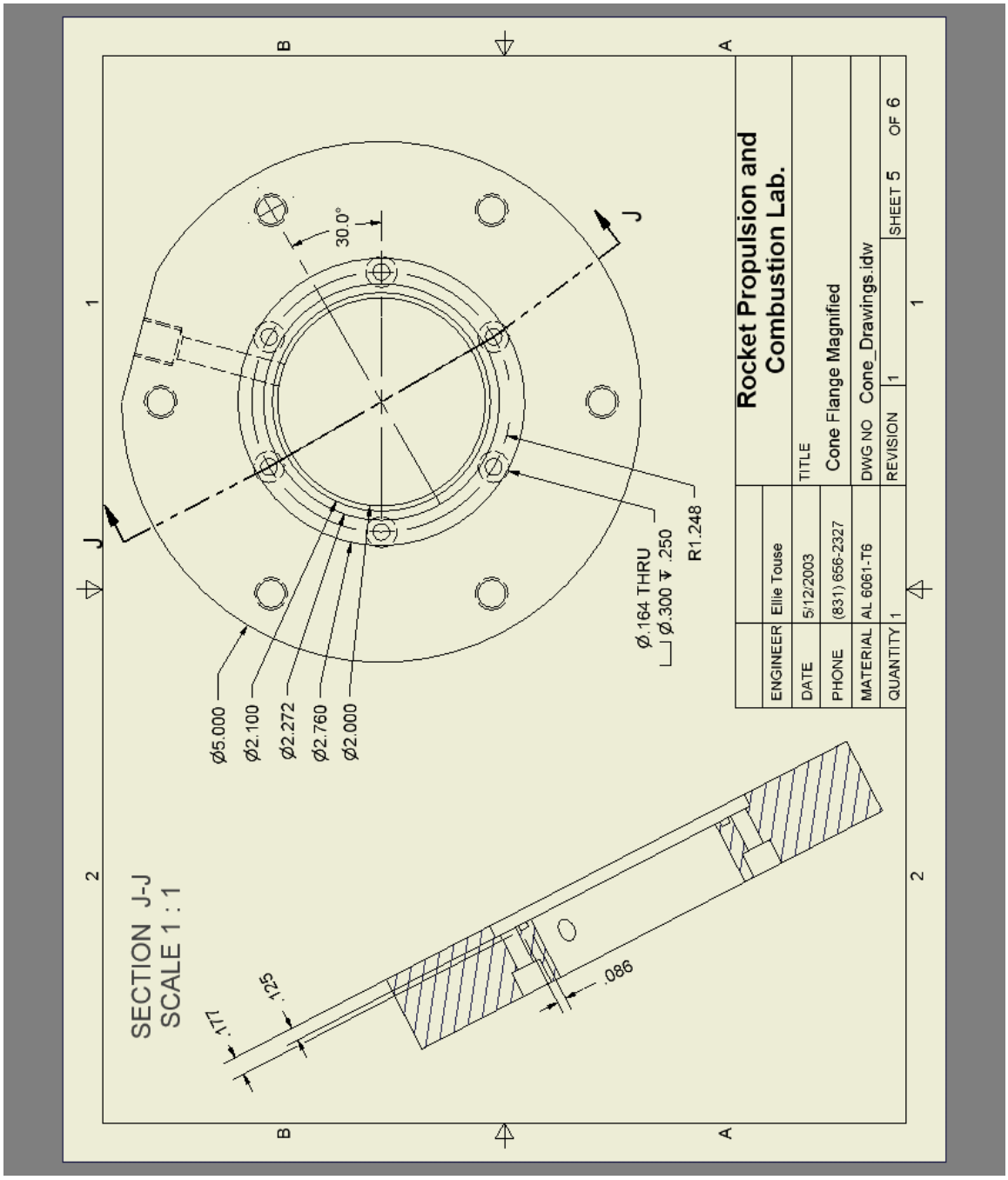

Figure 27 Cone Flange for Axisymmetric Test Section (Drawing 2 of 3)

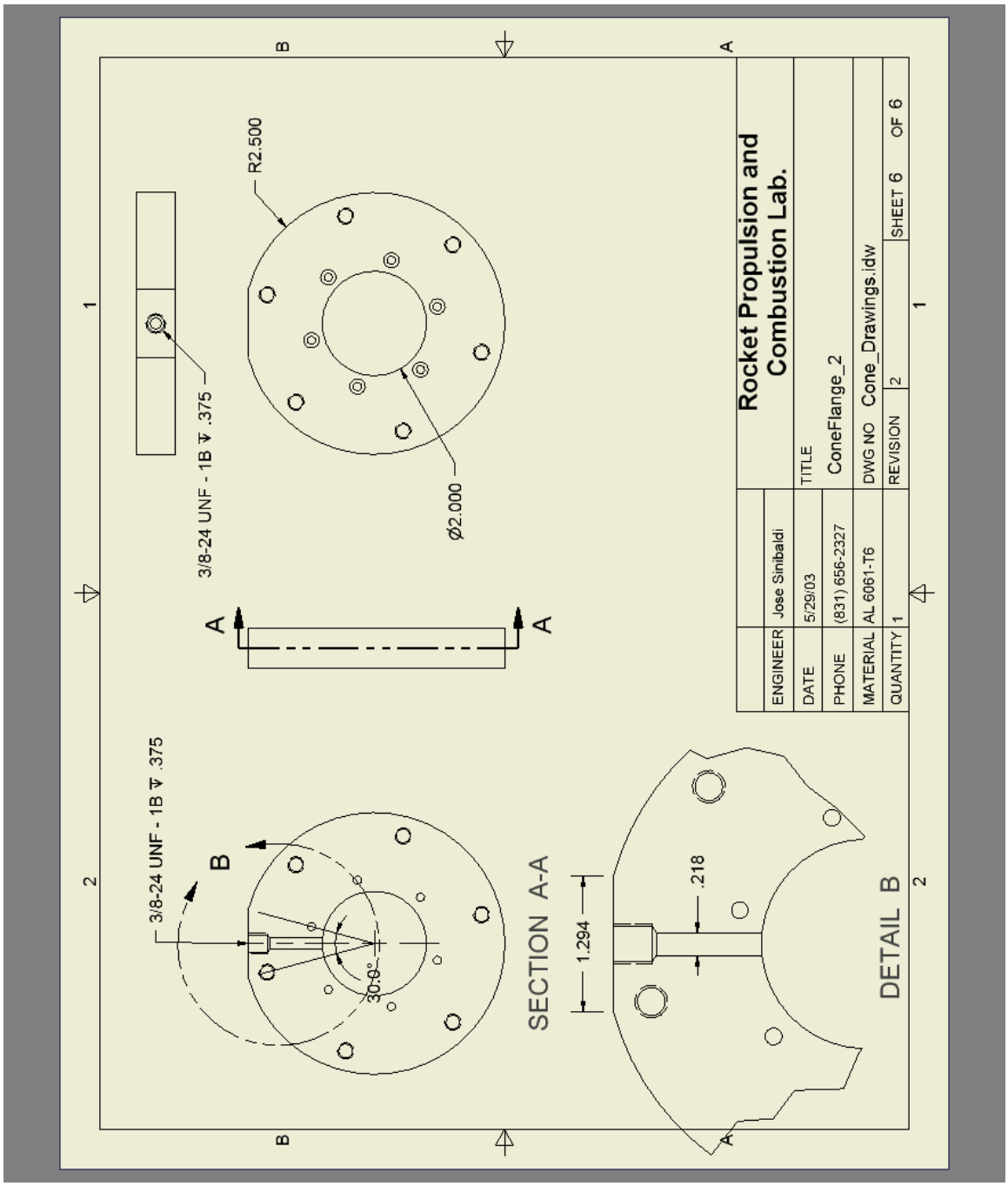

Figure 28 Cone Flange for Axisymmetric Test Section (Drawing 3 of 3)

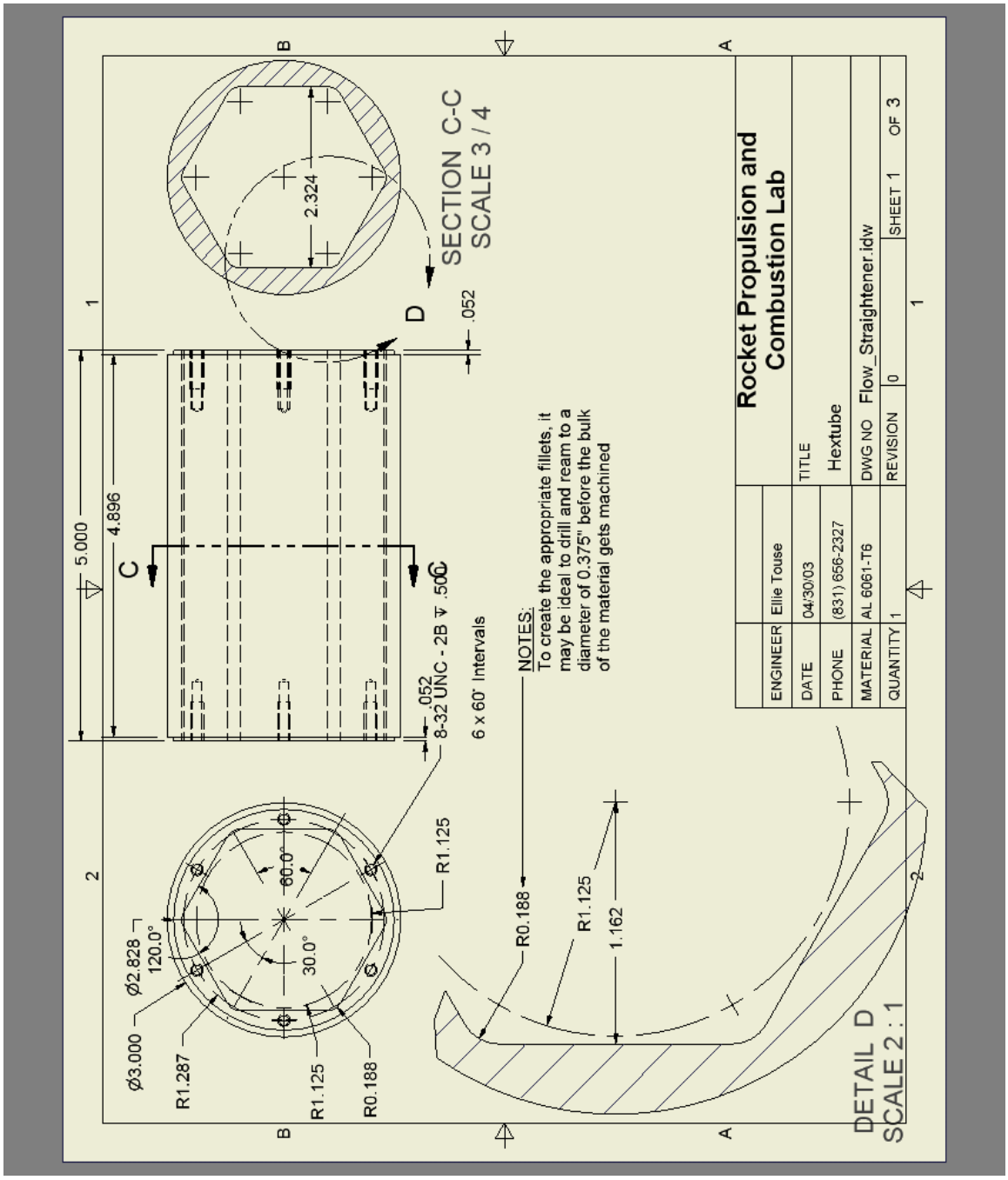

Figure 29 Flow Straightener Tube for Axisymmetric Test Section

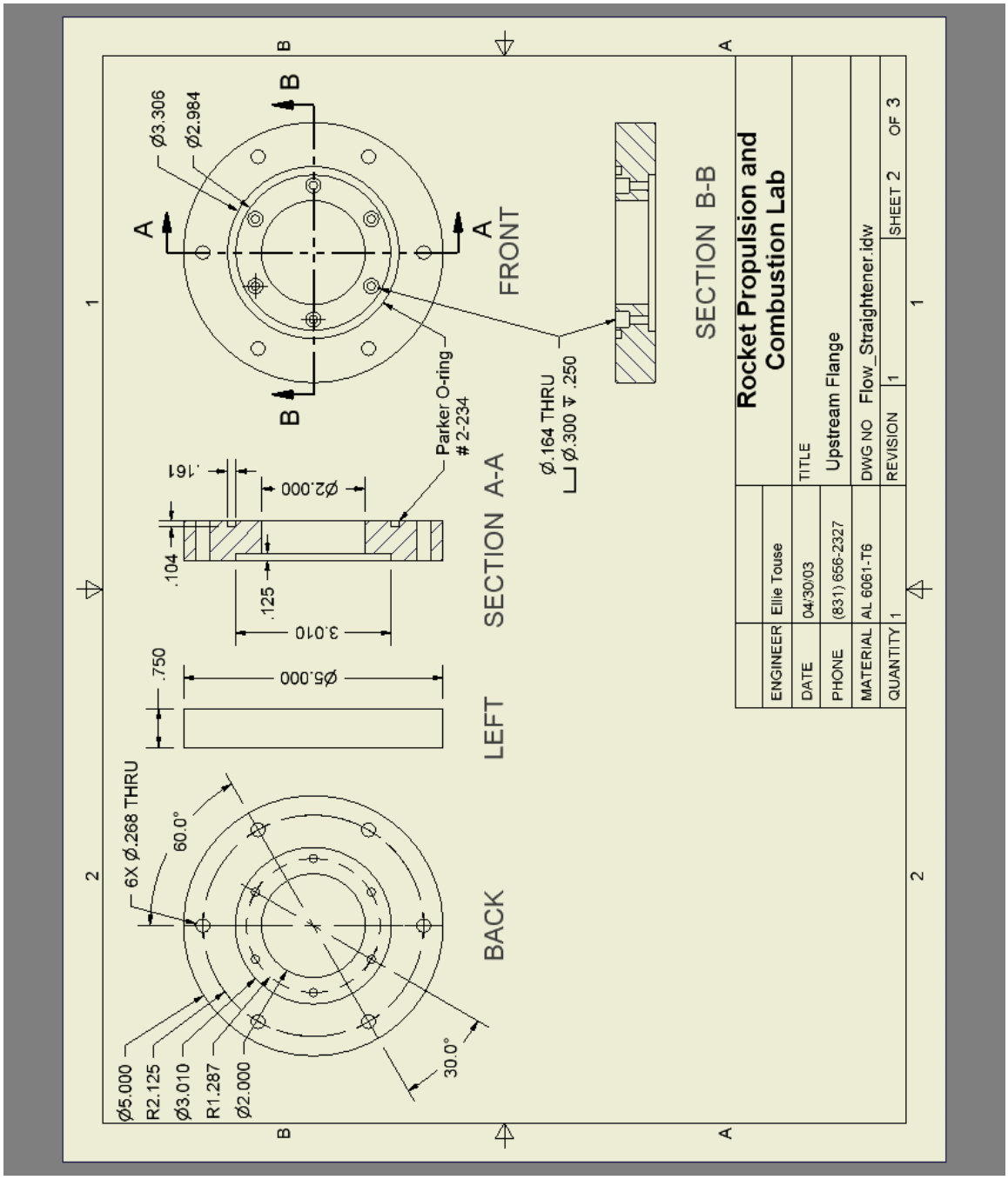

Figure 30 Flow Straightener Upstream Flange for Axisymmetric Test Section

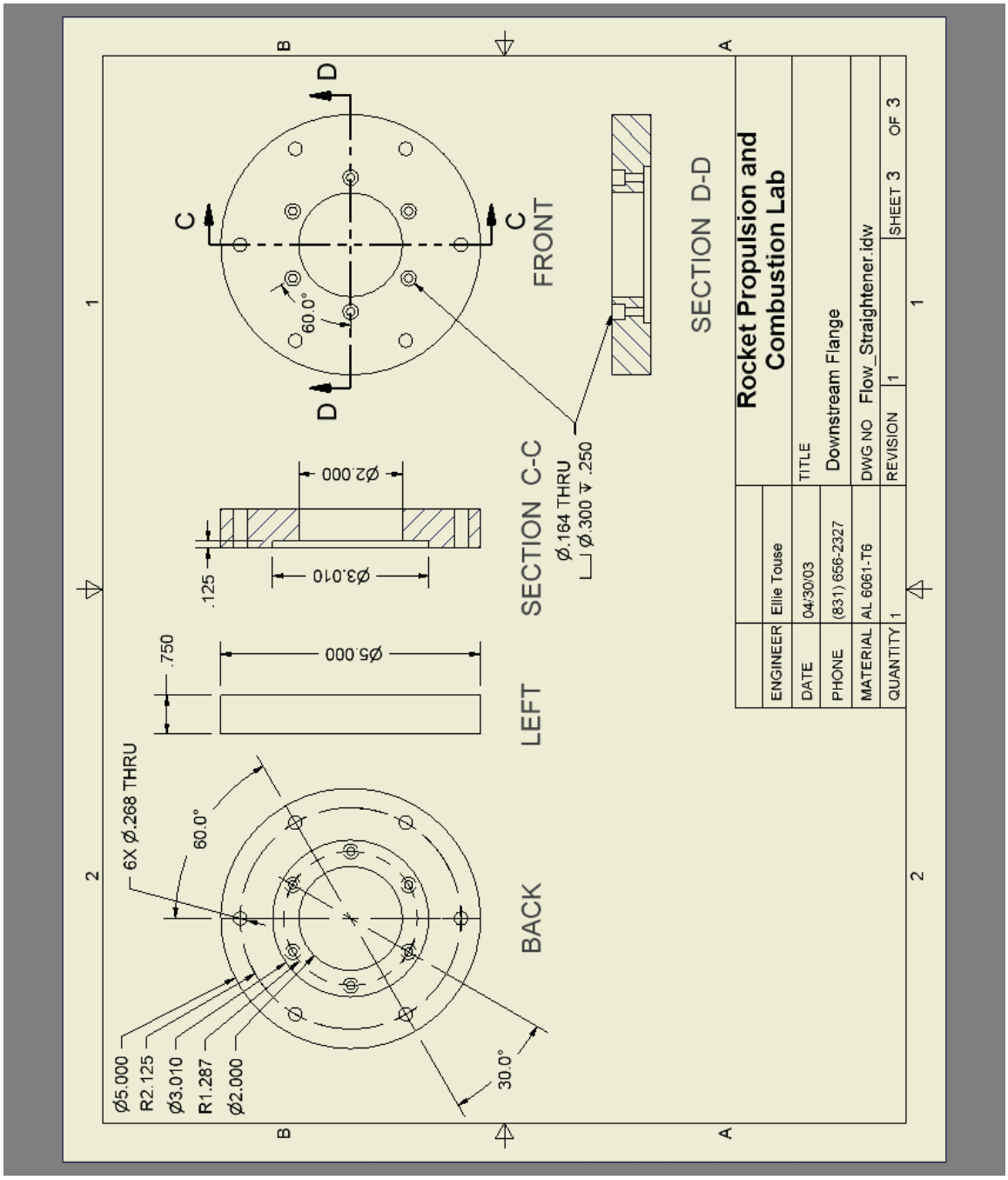

Figure 31 Flow Straightener Downstream Flange for Axisymmetric Test Section

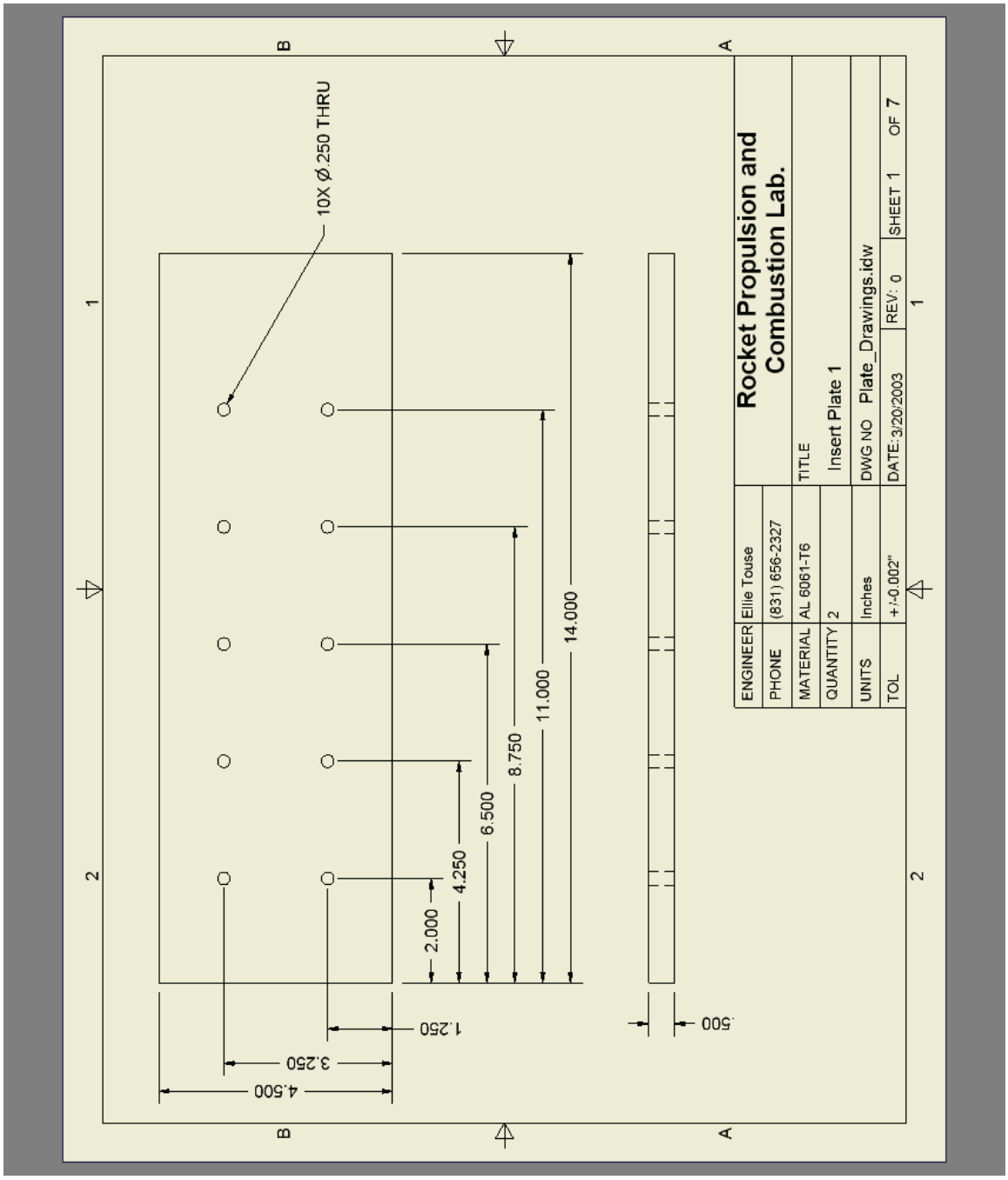

Figure 32 Insert Plate 1 for Transition Section of Two-Dimensional Test Section

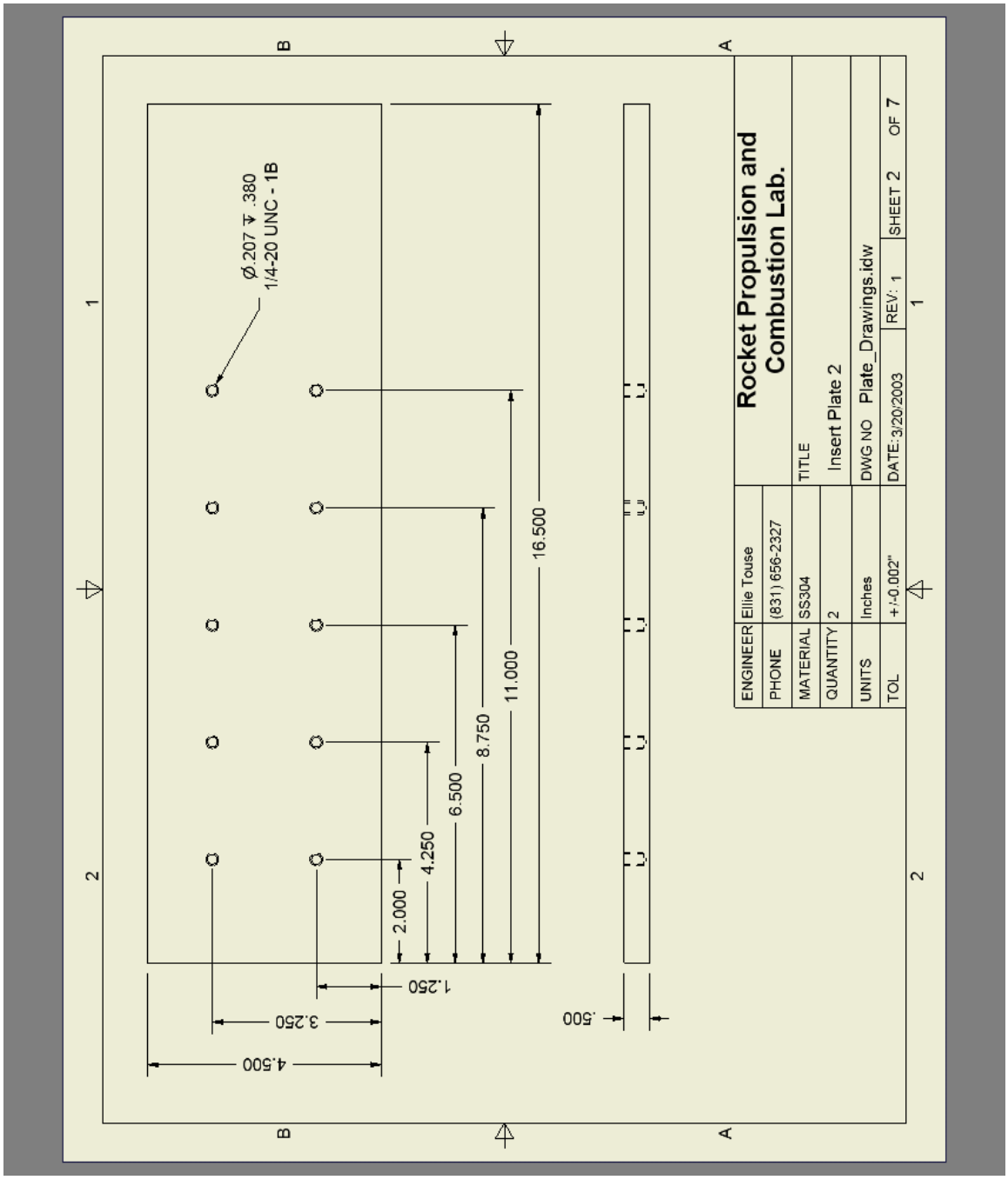

Figure 33 Insert Plate 2 for Transition Section of Two-Dimensional Test Section

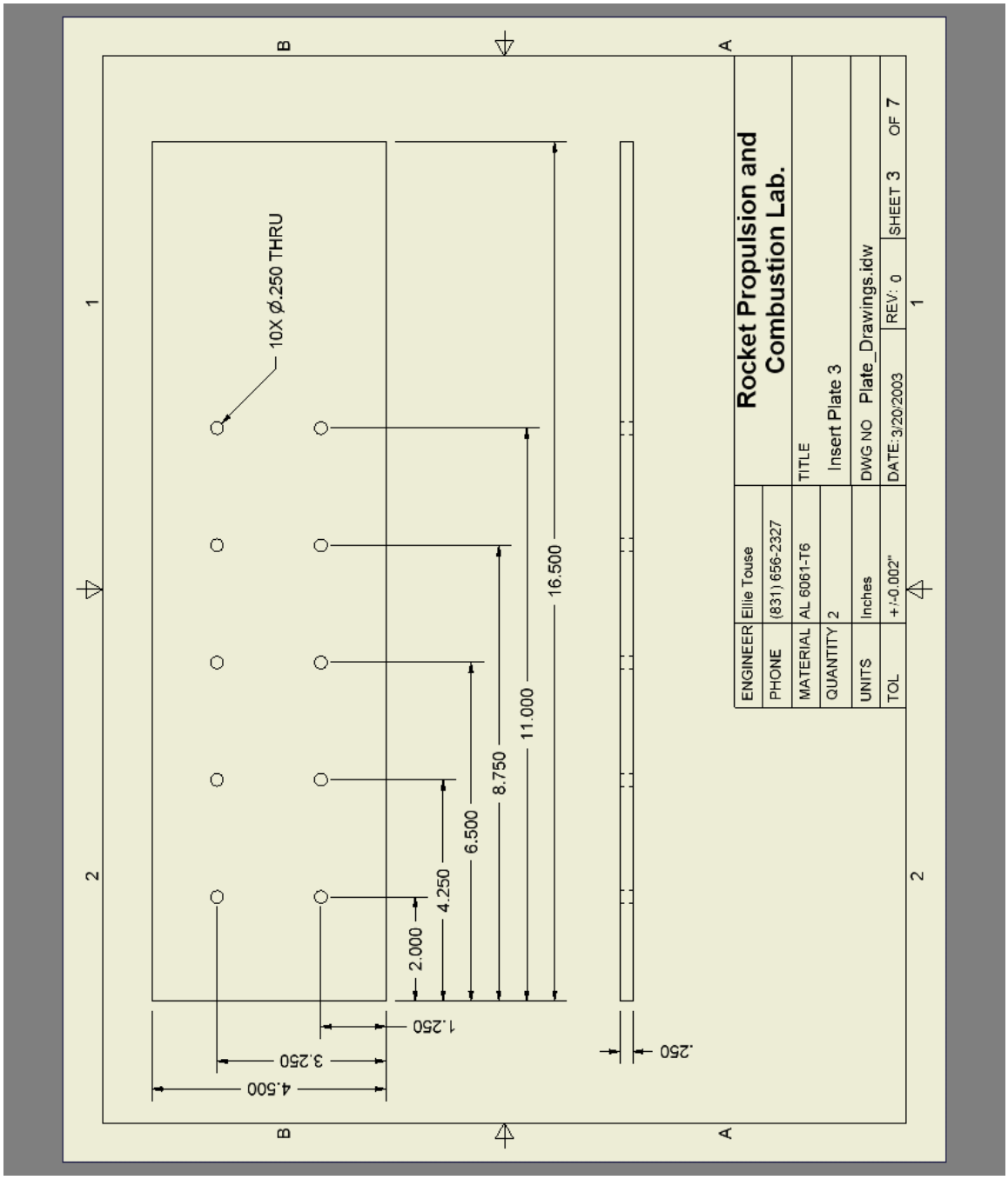

Figure 34 Insert Plate 3 for Transition Section of Two-Dimensional Test Section

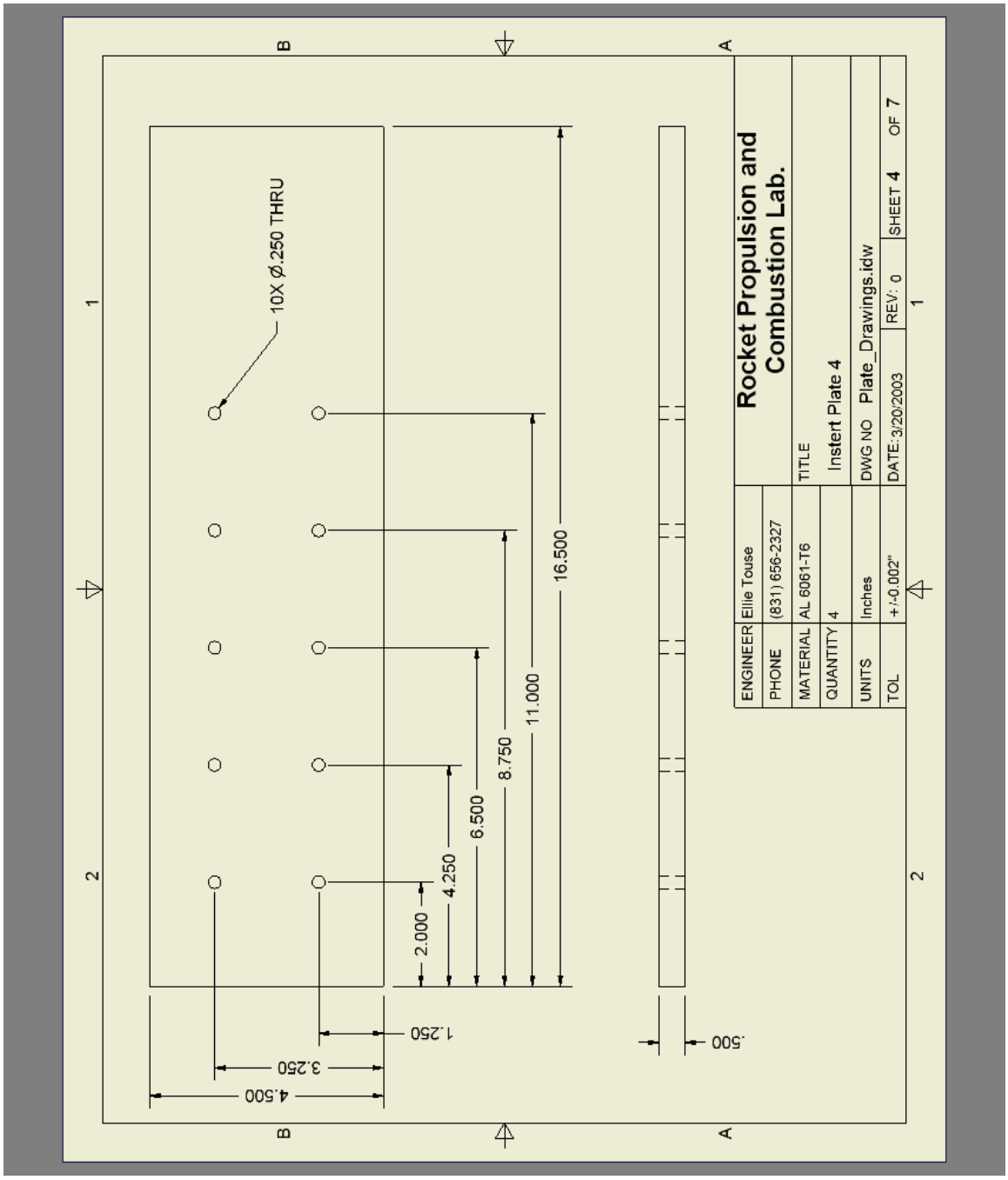

Figure 35 Insert Plate 4 for Transition Section of Two-Dimensional Test Section

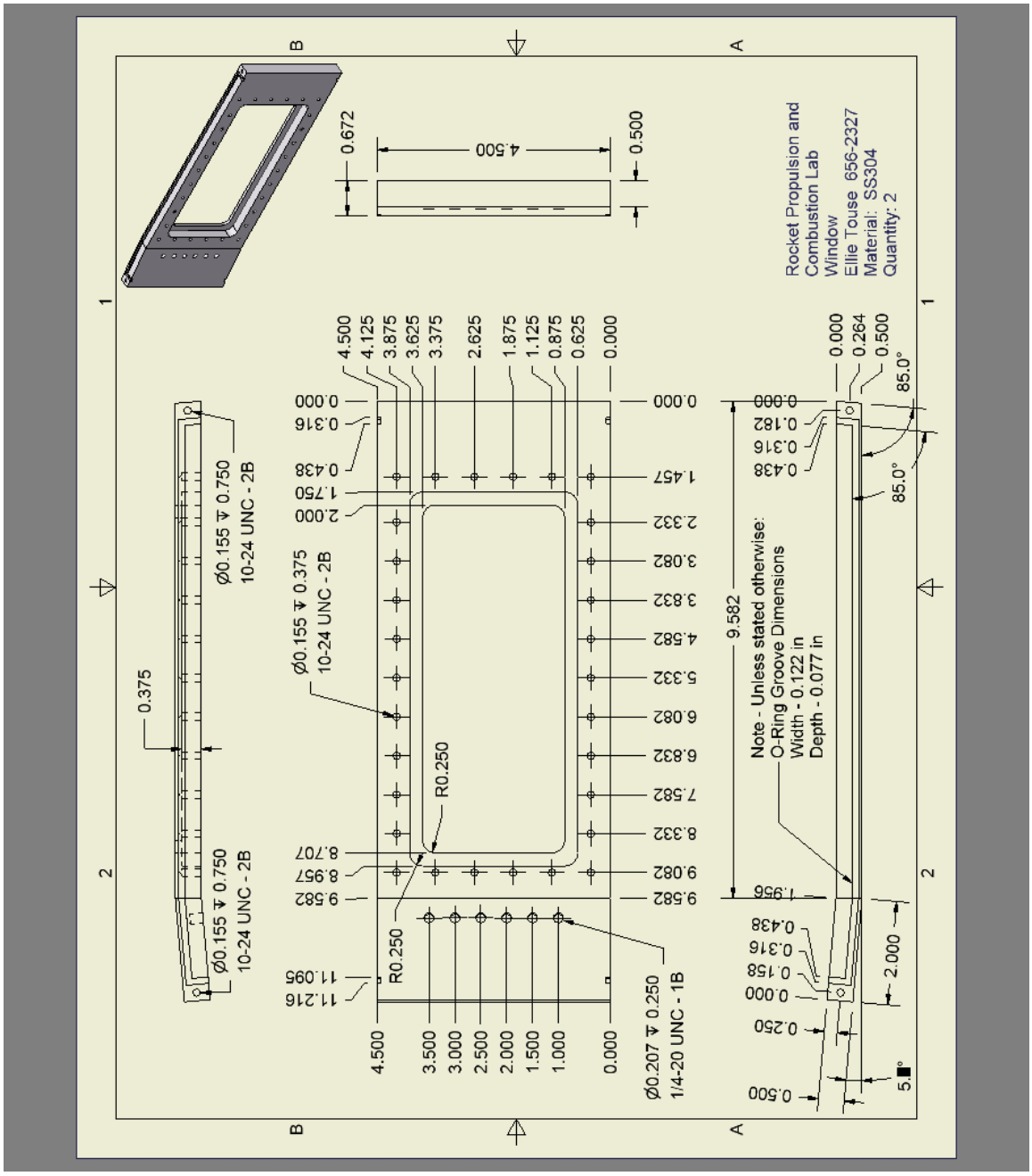

Figure 36 Injector Plate Frame for Optical Section of Two-Dimensional Test Section, Modified to Accommodate Support Brackets

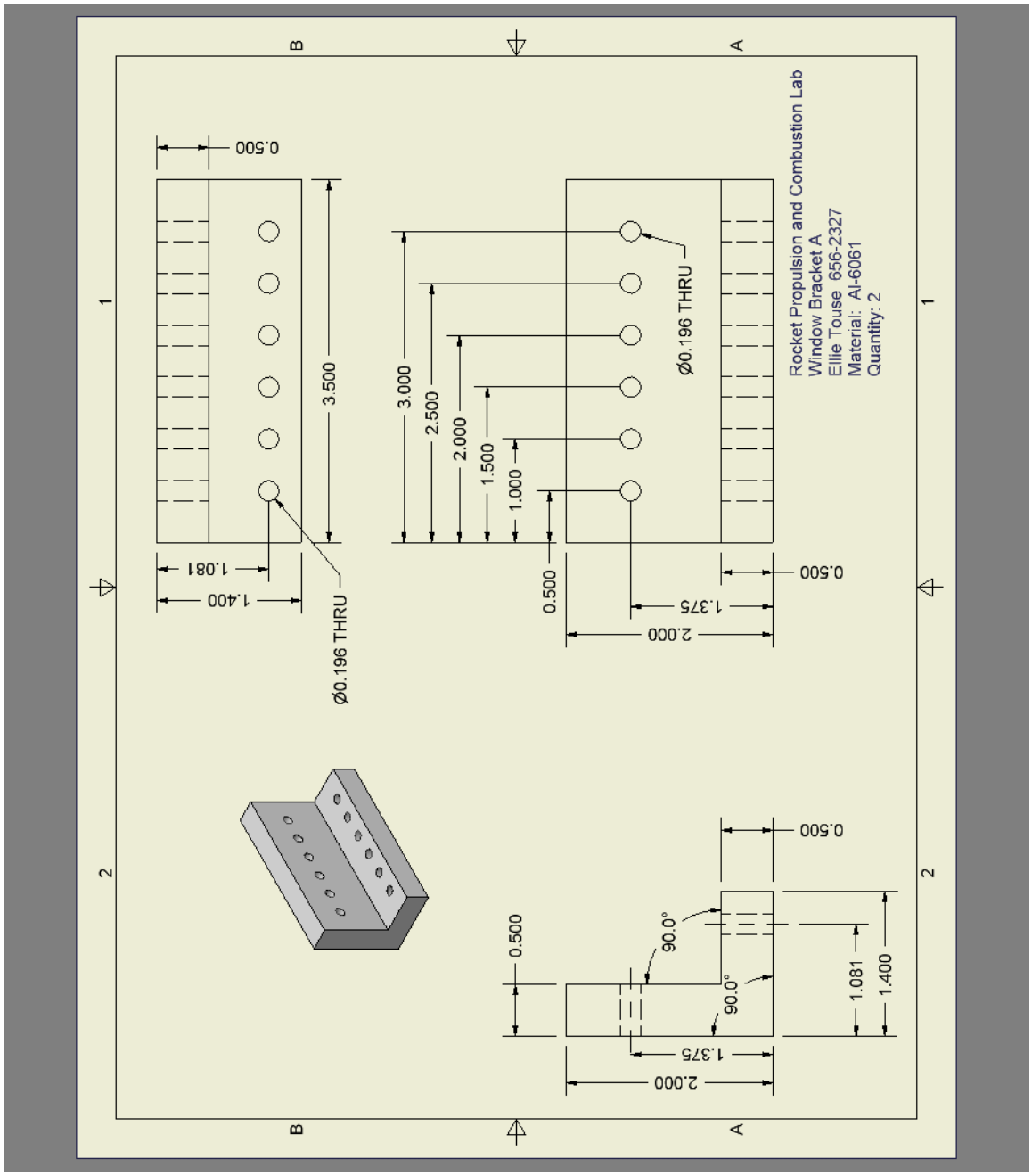

Figure 37 Support Bracket A for Injector Plate Frame used in Optical Section of Two-Dimensional Test Section

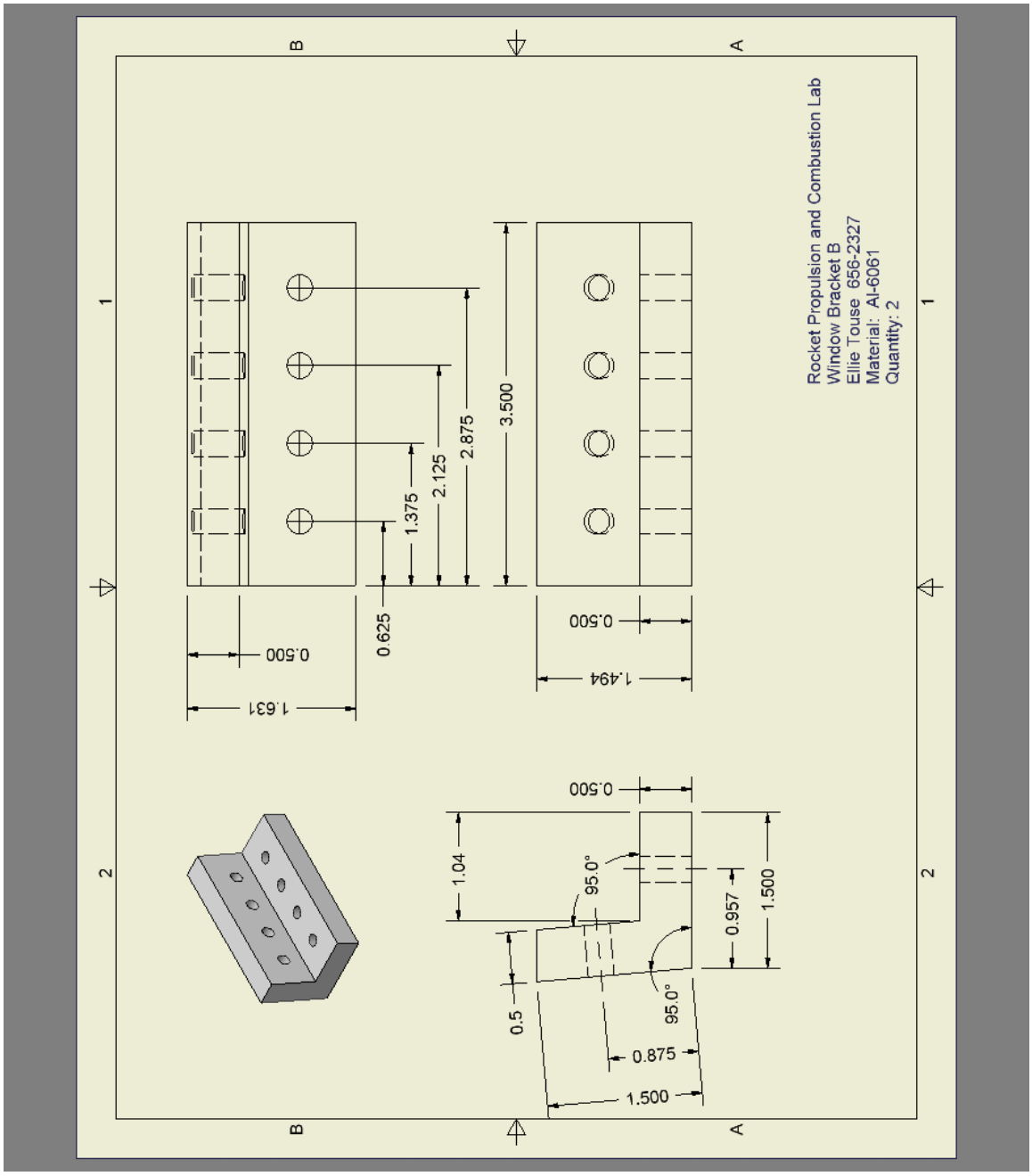

Figure 38 Support Bracket B for Injector Plate Frame used in Optical Section of Two-Dimensional Test Section

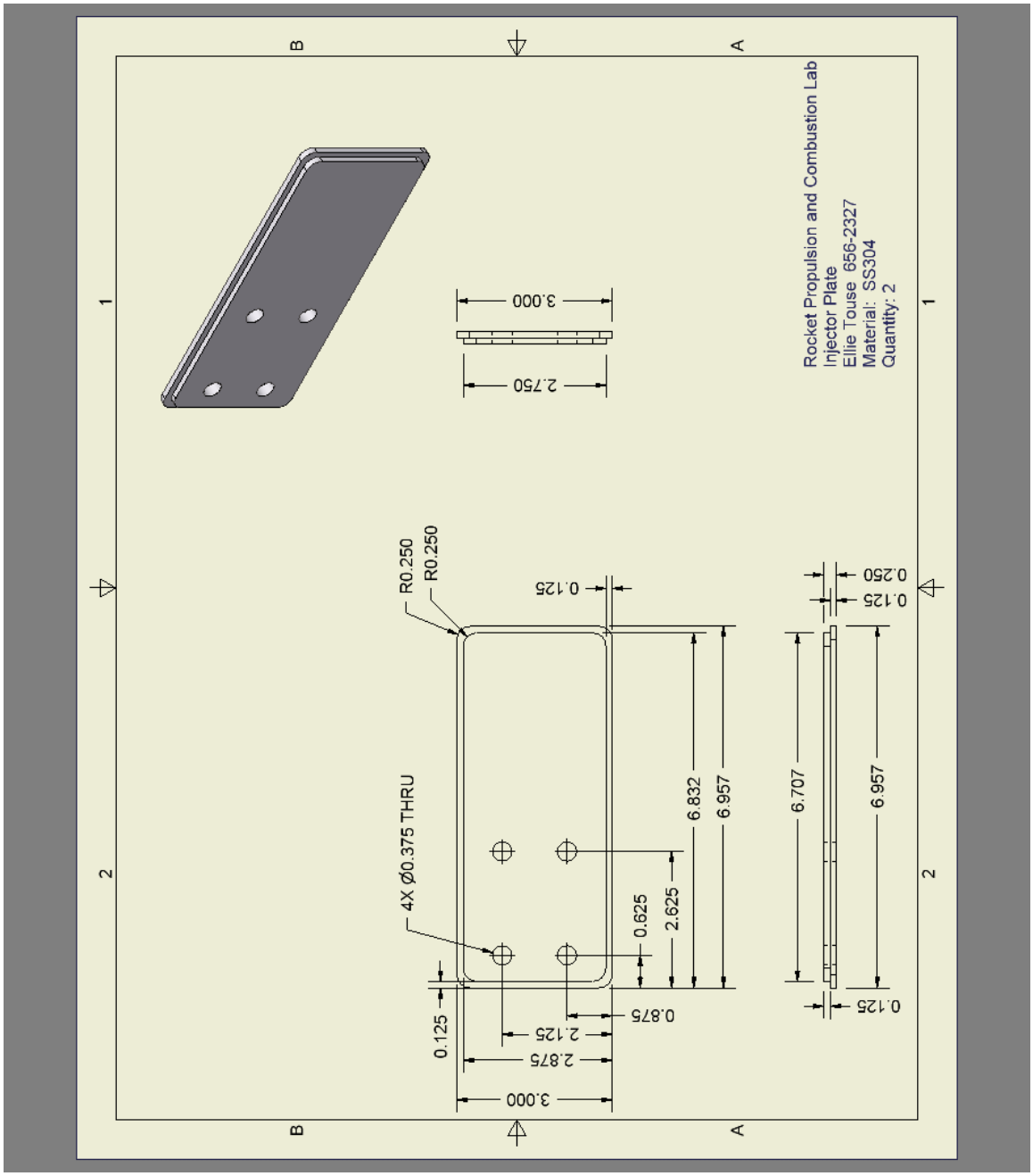

Figure 39 Injector Plate for Two-Dimensional Test Section, Modified to Accommodate 5-degree Wedge

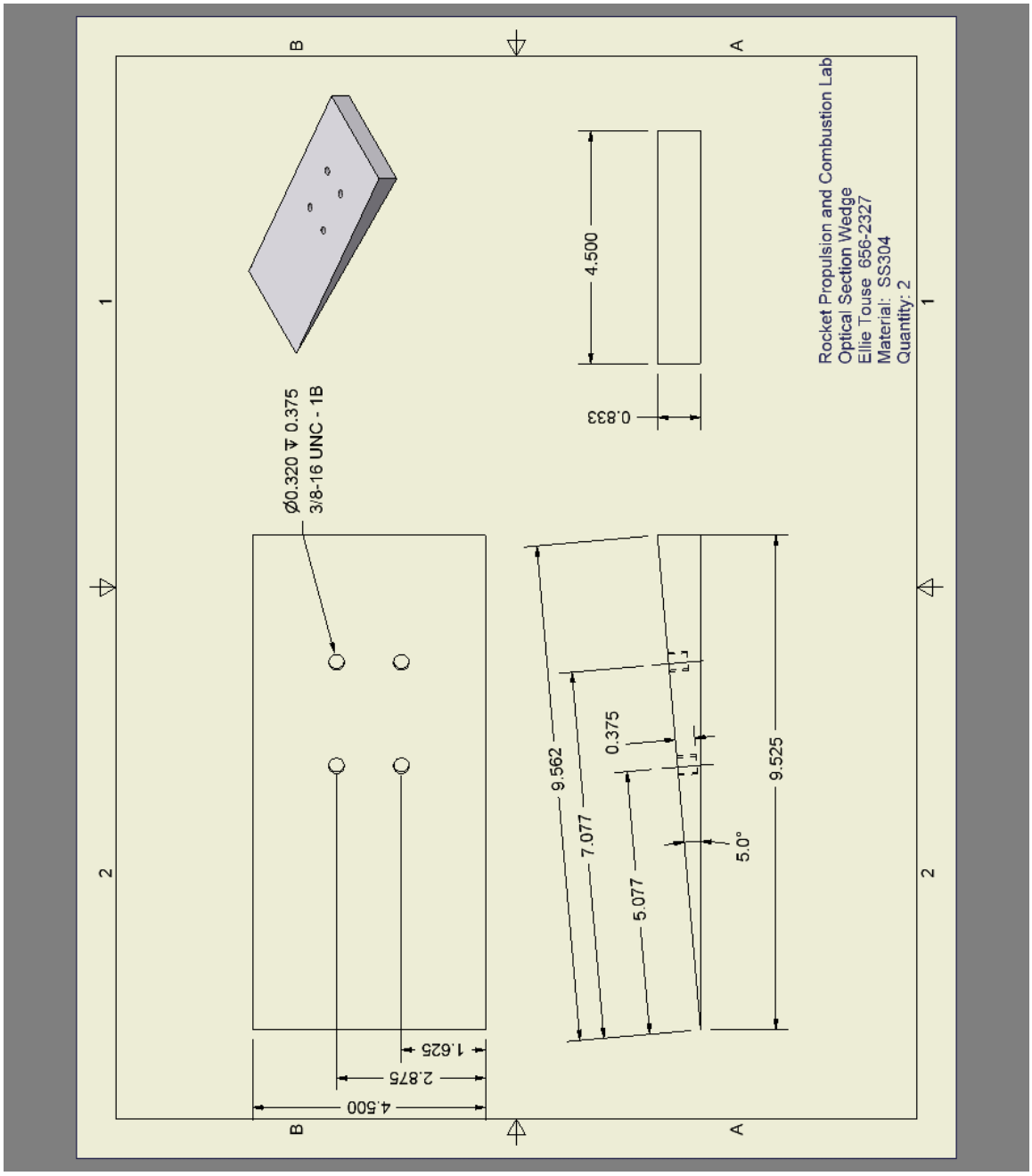

Figure 40 5-degree Wedge used in Optical Section of Two-Dimensional Test Section

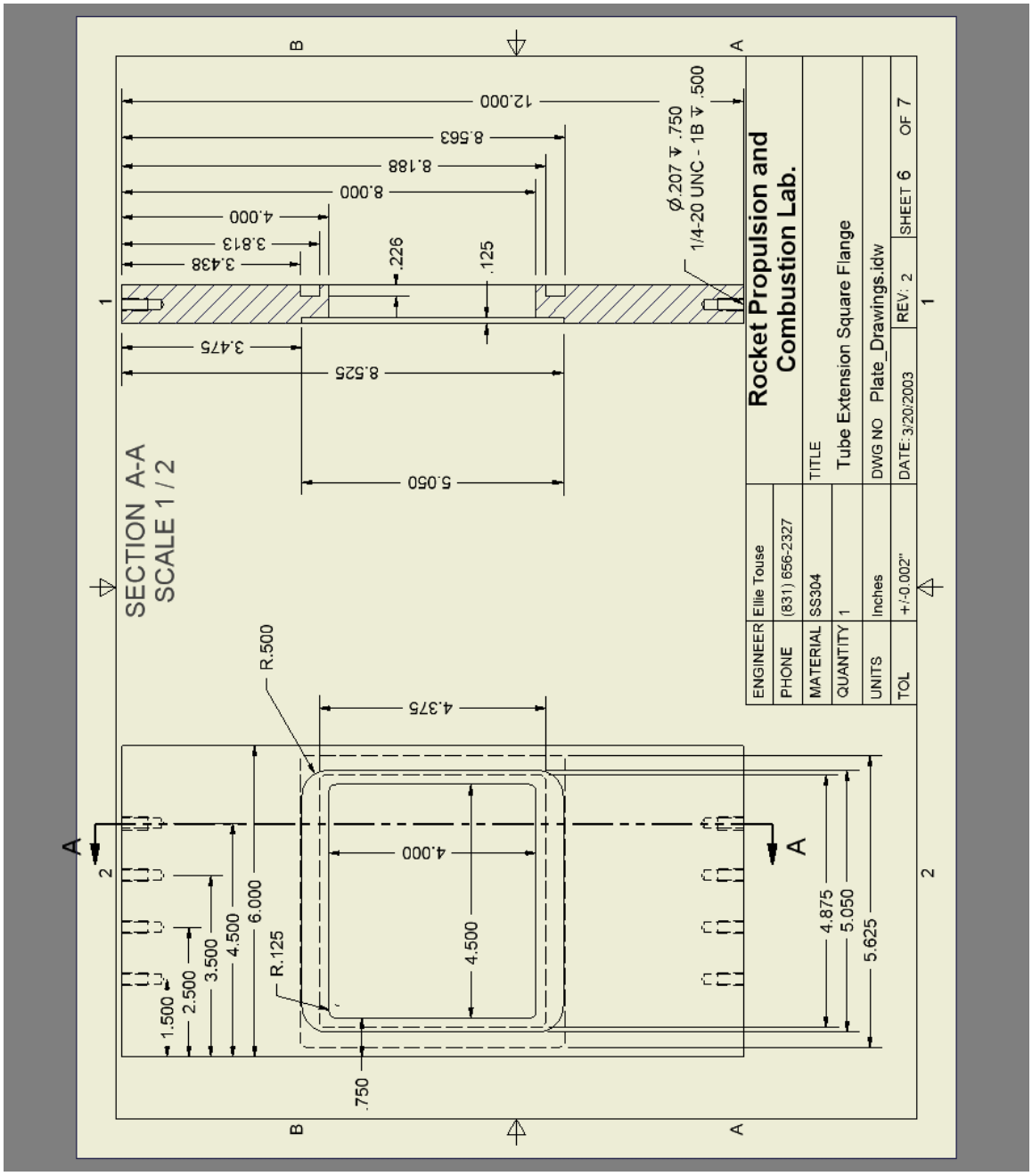

Figure 41 Flange for Tube Extension of Two-Dimensional Test Section

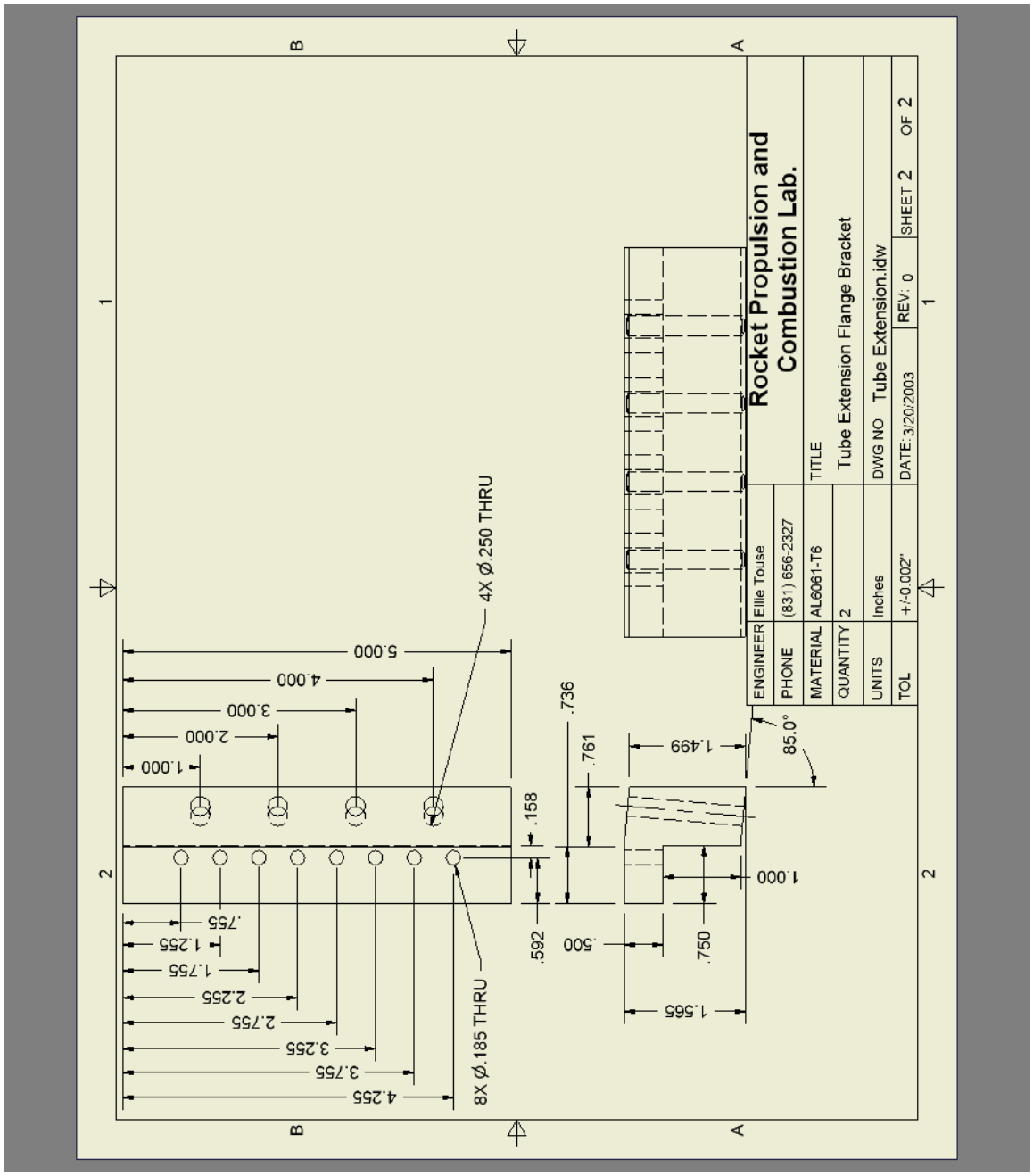

Figure 42 Brackets to Connect Tube Extension Flange to the Exit of the Optical Section of the Two-Dimensional Test Section

APPENDIX C. AXISYMMETRIC DATA

Equivalence ratio data																
Run #	t_f/a	t_f/o	DAQ(MHz)	P_f(psi)	P_ox(psi)	P_a(psi)	t_p1 (us)	t_p2 (us)	t_p3 (us)	t_p4 (us)	t_p5 (us)	Phi_fo	Phi_fa	Vfo(km/s)	Vfa(km/s)
030319_4	1.500	0.809	1.000	200	157	230	1958	2185	2254	2695	2736	0.9	1.0	2.209	1.859
030319_5	1.500	0.809	1.000	200	157	230	604	831	900	1333	1375	0.9	1.0	2.209	1.814
030319_6	1.500	0.809	1.000	200	157	230	354	581	648	1093	1135	0.9	1.0	2.275	1.814
030319_10	1.500	0.745	1.000	200	177	230	3166	3398	3469	3915	3956	0.8	1.0	2.146	1.859
030319_11	1.500	0.745	1.000	200	177	230	5672	5905	5974	6418	6460	0.8	1.0	2.209	1.814
030319_12	1.500	0.745	1.000	200	177	230	4174	4464	4533	4966	5007	0.8	1.0	2.209	1.859
030319_18	1.500	0.644	1.000	200	213	250	3285	3529	3601	4293	4376	0.7	1.0	2.117	0.918
030319_19	1.500	0.644	1.000	200	213	250	3337	3579	3650	4141	4183	0.7	1.0	2.146	1.814
030319_20	1.500	0.644	1.000	200	213	250	534	776	847	1542	1625	0.7	1.0	2.146	0.918
030319_20	1.500	0.644	1.000	200	213	250	758	996	1067	1712	1783	0.7	1.0	2.146	1.073
030327_4	1.500	0.851	1.000	200	145	245	7346	7572	7636	8070	8113	1.0	1.0	2.381	1.772
030327_5	1.500	0.851	1.000	200	145	245	7144	7369	7431	7855	7898	1.0	1.0	2.458	1.772
030327_6	1.500	0.851	1.000	200	145	245	3271	3490	3557	4004	4045	1.0	1.0	2.275	1.859
030327_10	1.500	0.969	1.000	200	120	245	4902	5116	5181	5612	5652	1.2	1.0	2.345	1.905
030327_11	1.500	0.969	1.000	200	120	245	3121	3334	3398	3825	3867	1.2	1.0	2.381	1.814
030327_12	1.500	0.969	1.000	200	120	245	3002	error	3280	3695	3737	1.2	1.0	no data	1.814
030327_16	1.500	1.084	1.000	200	98	245	2047	2289	2316	2733	2775	1.4	1.0	5.644	1.814
030327_17	1.500	1.084	1.000	200	98	245	897	1104	1168	1589	1631	1.4	1.0	2.381	1.814
030327_18	1.500	1.084	1.000	200	98	245	2432	2638	2701	3123	3166	1.4	1.0	2.419	1.772
030327_22	1.500	1.174	1.000	200	86	245	3313	3515	3576	3992	4034	1.6	1.0	2.498	1.814
030327_23	1.500	1.174	1.000	200	86	245	6873	7074	7135	7552	7594	1.6	1.0	2.498	1.814
030327_24	1.500	1.174	1.000	200	86	245	5862	6063	6124	6540	6583	1.6	1.0	2.498	1.772
030327_28	1.500	1.26	1.000	200	75	245	7044	7242	7303	7723	7768	1.8	1.0	2.498	1.693
030327_29	1.500	1.26	1.000	200	75	245	4888	5087	5149	5568	5612	1.8	1.0	2.458	1.732
030327_30	1.500	1.26	1.000	200	75	245	765	962	1023	1442	1484	1.8	1.0	2.498	1.814
030327_34	1.500	1.364	1.000	200	65	245	4587	4784	4844	5262	5304	2.0	1.0	2.540	1.814
030327_35	1.500	1.364	1.000	200	65	245	7470	7714	7773	8186	8228	2.0	1.0	2.583	1.814
030327_36	1.500	1.364	1.000	200	65	245	8258	8500	8560	8971	9014	2.0	1.0	2.540	1.772
030331_4	1.500	1.103	1.000	250	84	307	3975	4172	4232	4650	4693	2.0	1.0	2.540	1.772
030331_5	1.500	1.103	1.000	250	84	307	4047	4243	4304	4724	4766	2.0	1.0	2.498	1.814
030331_6	1.500	1.103	1.000	250	84	307	3074	3272	3333	3756	3798	2.0	1.0	2.498	1.814
030331_10	1.500	1.185	1.000	250	73	307	4514	4754	4815	5226	5269	2.2	1.0	2.498	1.772
030331_11	1.500	1.185	1.000	250	73	307	3359	3600	3660	4077	4119	2.2	1.0	2.540	1.814
030331_12	1.500	1.185	1.000	250	73	307	5458	5700	5760	6175	6218	2.2	1.0	2.540	1.772
030331_16	1.500	1.221	1.000	250	68	307	7576	7816	7877	8292	8333	2.4	1.0	2.498	1.859
030331_17	1.500	1.221	1.000	250	68	307	1959	2201	2261	2677	2720	2.4	1.0	2.540	1.772
030331_18	1.500	1.221	1.000	250	68	307	4170	4410	4470	4891	4930	2.4	1.0	2.540	1.954
030331_22	1.500	1.21	1.000	250	66	326	5782	6068	6109	6511	6552	2.6	1.0	3.717	1.859
030331_23	1.500	1.21	1.000	250	66	326	1743	2010	2068	2471	2514	2.6	1.0	2.628	1.772
030331_24	1.500	1.21	1.000	250	66	326	5011	5251	5312	5724	5764	2.6	1.0	2.498	1.905
030401_4	1.500	1.256	1.000	250	63	315	2639	2875	2936	3351	3394	2.6	1.0	2.498	1.772
030401_5	1.500	1.224	1.000	250	65	315	938	1178	1238	1652	1696	2.6	1.0	2.540	1.732
030401_6	1.500	1.224	1.000	250	65	315	2552	2792	2851	3265	3307	2.6	1.0	2.583	1.814
030401_10	1.500	1.311	1.000	250	57	315	2391	2629	2687	3094	3137	2.8	1.0	2.628	1.772
030401_11	1.500	1.129	1.000	300	69	364	1388	1687	1709	2109	2151	2.8	1.0	6.927	1.814
030401_12	1.500	1.129	1.000	300	69	364	2518	2795	2852	3252	3293	2.8	1.0	2.674	1.859
030401_16	1.500	1.162	1.000	300	63	364	5251	5517	5571	5972	6013	3.0	1.0	2.822	1.859
030401_17	1.500	1.162	1.000	300	63	364	8347	8600	8657	9056	9099	3.0	1.0	2.674	1.772
030401_18	1.500	1.162	1.000	300	63	364	5836	6132	6189	6588	6630	3.0	1.0	2.674	1.814
030401_22	1.500	1.24	1.000	300	56	364	No Detonation					3.2	1.0	no data	no data
030401_26	1.500	1.181	1.000	300	61	364	No Detonation					3.1	1.0	no data	no data

Table 2. Axisymmetric Equivalence Ratio Data

Axisymmetric Nitrogen Dilution Data

case#	phi_ox	phi_air	N2p	Temp	mf_ox	mf_air	ts1_min	P1max	ts4_min	P4max	DT1	DT2	Ispf
	NA	NA	NA	(K)	(kg)	(kg)	(us)	(Pa)	(us)	(Pa)	(us)	(us)	(s)
R030718_21	1.0	1.0	0.10	285	0.002735	0.000517	0.00185	4571725.26	0.002465	2712525.96	0.004435	0.002515	459.139871
R030718_22	1.0	1.0	0.10	285	0.002735	0.000517	0.00433	4663278.70	0.004675	2535365.79	0.00438	0.00302	520.868159
R030718_23	1.0	1.0	0.10	285	0.002735	0.000517	0.007635	5142600.12	0.00812	2729146.75	0.004305	0.002695	474.228606
R030718_24	1.0	1.0	0.20	285	0.002495	0.000517	0.005955	5704012.03	0.00632	2084167.64	0.005035	0.00341	639.851061
R030718_25	1.0	1.0	0.20	285	0.002495	0.000517	0.0021	4452707.45	0.00262	2613640.82	0.005825	0.00479	538.228672
R030718_26	1.0	1.0	0.20	285	0.002495	0.000517	0.00883	4042005.89	0.009195	2434522.73	0.00409	0.002815	519.252312
R030718_27	1.0	1.0	0.30	285	0.002242	0.000517	0.00195	8014937.59	0.002365	2063405.81	0.00452	0.00257	629.871691
R030718_28	1.0	1.0	0.40	285	0.001975	0.000517	0.00784	4208916.12	0.00872	2916227.79	0.004785	0.00324	644.979226
R030718_29	1.0	1.0	0.35	285	0.00211	0.000517	0.00649	3327752.91	0.00714	2929152.05	0.005325	0.0033	677.504843
R030718_30	1.0	1.0	0.40	285	0.001975	0.000517	0.00131	4983537.90	0.001935	2687462.39	0.00803	0.00288	621.840986
R030721_2	1.0	1.0	0.45	285	0.001836	0.000517	0.00855	13153325.66	0.00969	6451090.34	0.00498	0.002405	589.673373
R030721_3	1.0	1.0	0.45	285	0.001836	0.000517	0.00415	11549095.95	0.00542	4134601.49	0.006735	0.00252	565.019684
R030721_4	1.0	1.0	0.45	285	0.001836	0.000517	0.005275	5038436.15	0.00642	5052920.33	0.005235	0.0024	671.428469
R030721_5	1.0	1.0	0.50	285	0.001693	0.000517	0.0036	6793907.69	0.004825	5451270.68	0.00565	0.003045	776.588896
R030721_6	1.0	1.0	0.50	285	0.001693	0.000517	0.007925	9637916.83	0.009105	9105713.68	0.004825	0.00272	612.93342
R030721_7	1.0	1.0	0.50	285	0.001693	0.000517	0.0041	17999760.20	0.00534	4840871.95	0.0065	0.00252	704.332613
R030721_8	1.0	1.0	0.55	285	0.001546	0.000517	0.006065	9654990.57	0.007365	18696971.90	0.00553	0.002985	791.564322
R030721_9	1.0	1.0	0.55	285	0.001546	0.000517	0.00869	12233046.92	0.009905	4811301.89	0.00501	0.002445	667.333701
R030721_10	1.0	1.0	0.55	285	0.001546	0.000517	0.005395	13549196.05	0.006635	5245849.92	0.00664	0.00393	770.081804
R030721_11	1.0	1.0	0.60	285	0.001394	0.000517	0.005395	7996152.69	0.006685	4293195.28	0.00582	0.00295	761.291846
R030721_12	1.0	1.0	0.60	285	0.001394	0.000517	0.00633	19072343.17	0.007615	3415246.16	0.00446	0.002815	543.771552
R030721_13	1.0	1.0	0.60	285	0.001394	0.000517	0.00306	16511230.91	0.004315	3373854.49	0.005175	0.00393	606.556095
R030721_14	2.4	1.0	0.50	285	0.001858	0.000517	0.00403	10150729.57	0.00467	2859413.93	0.004185	0.00248	629.265566
R030721_15	2.4	1.0	0.50	285	0.001858	0.000517	0.00774	10674615.96	0.00837	2969349.42	0.004155	0.002615	550.756652
R030721_16	2.4	1.0	0.50	285	0.001858	0.000517	0.009405	16882387.00	0.010705	2667523.07	0.00488	0.00207	580.859641
R030721_17	2.4	1.0	0.50	285	0.001858	0.000517	0.00731	4876629.58	0.00819	6486549.32	0.006065	0.003105	687.348424
R030721_18	2.4	1.0	0.60	285	0.001576	0.000517	0.025085	1344104.40	0.00819	1298455.66	0.003425	0.018635	370.874584
R030721_19	2.4	1.0	0.55	285	0.001721	0.000517	0.01269	918290.40	0.011755	6187639.63	0.00358	0.002655	352.340787
R030721_20	2.4	1.0	0.55	285	0.001721	0.000517	0.012855	934020.32	0.011805	14588807.12	0.00348	0.00272	456.930258
R030721_21	2.4	1.0	0.45	285	0.001987	0.000517	0.006605	1803115.28	0.007205	3145114.79	0.005475	0.00279	602.611332
R030721_22	2.4	1.0	0.45	285	0.001987	0.000517	0.003465	2343040.74	0.004055	2672111.27	0.00585	-0.00405	730.093957
R030721_23	2.4	1.0	0.45	285	0.001987	0.000517	0.0052	3522095.80	0.005775	3530670.38	0.00442	0.002205	594.07114
R030721_24	1.5	1.0	0.45	285	0.001897	0.000517	0.00598	4384421.96	0.00666	7393811.96	0.00442	0.002685	737.737528
R030721_25	1.5	1.0	0.50	285	0.001759	0.000517	0.006145	4883736.36	0.006665	3328348.39	0.00482	0.003635	922.249277
R030721_26	1.5	1.0	0.55	285	0.001615	0.000517	0.004735	19368749.44	0.00589	3747647.64	0.00535	0.002765	861.720943
R030721_27	1.5	1.0	0.60	285	0.001466	0.000517	0.004435	13388076.72	0.005965	2840952.35	0.005375	0.00214	745.025617
R030721_28	1.5	1.0	0.65	285	0.00131	0.000517	0.004435	2678830.41	0.00746	3508290.90	0.00722	0.002545	683.137276
R030722_1	2.0	1.0	0.45	285	0.001949	0.000517	0.008845	9815951.18	0.00948	2935416.57	0.00419	0.01051	784.371158
R030722_2	2.0	1.0	0.45	285	0.001949	0.000517	0.00243	9243443.87	0.002995	2097566.57	0.004255	0.016995	753.2549155
R030722_3	2.0	1.0	0.45	285	0.001949	0.000517	0.00336	8859357.46	0.004145	9137442.90	0.004335	0.002755	745.205238
R030722_4	2.0	1.0	0.45	285	0.001949	0.000517	0.001625	8957829.51	0.002155	2443958.46	0.00502	0.00357	641.517031
R030722_5	2.0	1.0	0.50	285	0.001816	0.000517	0.00549	10115500.58	0.00636	9007476.69	0.00443	0.0026	641.517031
R030722_6	2.0	1.0	0.50	285	0.001816	0.000517	0.00266	9994763.20	0.003335	2942212.19	0.0049	0.003755	711.348984
R030722_7	2.0	1.0	0.50	285	0.001816	0.000517	0.00705	8183721.64	0.008175	5237802.60	0.004365	0.002645	611.540552
R030722_8	2.0	1.0	0.50	285	0.001816	0.000517	0.009105	9981659.41	0.00988	5950977.65	0.004345	0.00248	724.3552695
R030722_9	2.0	1.0	0.55	285	0.001677	0.000517	0.008015	10369109.69	0.009155	4117349.67	0.006295	0.0026	956.080433
R030722_10	2.0	1.0	0.55	285	0.001677	0.000517	0.00542	10201770.81	0.006565	7164983.83	0.0071	0.00376	868.7516745
R030722_11	2.0	1.0	0.55	285	0.001677	0.000517	0.005285	10221086.30	0.0065	5126391.36	0.00406	0.002595	593.658587
R030722_12	2.0	1.0	0.60	285	0.00153	0.000517	0.00543	2524615.04	0.006555	6324081.31	0.00483	0.002245	753.979272
R030722_13	2.0	1.0	0.60	285	0.00153	0.000517	0.00717	1355466.47	0.008295	8329222.50	0.00506	0.002245	684.4958785
R030722_14	2.0	1.0	0.60	285	0.00153	0.000517	0.00558	1470420.43	0.006585	6120252.23	0.005875	0.003555	797.0737405
R030722_15	2.0	1.0	0.65	285	0.001375	0.000517	0.010225	5395845.71	0.01154	3090914.56	0.004275	0.002865	368.1343555
R030722_16	2.0	1.0	0.65	285	0.001375	0.000517	0.010225	1122630.49	0.00635	3971867.27	0.00063	0.002755	293.5692815
R030722_17	2.0	1.0	0.65	285	0.001375	0.000517	0.00888	804051.86	0.009935	3506765.64	0.005195	0.00274	515.0419295

Table 3. Axisymmetric Nitrogen Dilution Data

APPENDIX D. MATLAB CODE

```
%*************************************************************
% Analyzes pressure channels 1 & 4 and generates Ispf plots for*
% a given list of files vs. phi_fuel-ox values inside the file *
% 'filename_phi2.txt'                                          *
%*************************************************************
clear all;
close all;

% Constants
Po       = 101325;
in2m     = 0.0254;
psi2Pa   = Po/14.696;
volt2psi = 300;
Temp     = 285;
R        = 8314.3;
phi_air  = 1.0;

dia1     = 2.0*in2m;
dia3     = 4.0*in2m;
L1       = 0.9144;
L3       = 0.8128;
A1       = 0.25*pi*dia1^2;
A3       = 0.25*pi*dia3^2 - A1;

% Cone Measurements
R_c=1*in2m;
L_c=7.225*in2m;
Vol_cone=(1/3)*pi*(R_c)^2*L_c;

% Flow Straightener Measurements
R_fs=1*in2m;
L_fs=5*in2m;
Vol_fs=pi*(R_fs)^2*L_fs;

Vol_1    = A1*L1+Vol_cone+Vol_fs;
Vol_3    = 0.25*pi*dia3^2*L3;
```

```
MW_C     = 12.011;
MW_O     = 15.994;
MW_N     = 14.0067;
MW_H     = 1.0079;
MW_N2    = 2*MW_N;
MW_O2    = 2*MW_O;
MW_fuel  = 2*MW_C + 4*MW_H;

%Initialize variables
i=1:30000;
ps1(i)=0;
ps3(i)=0;
ts1(i)=0;
ts3(i)=0;
It_1(i)=0;
It_3(i)=0;
Ispf(i)=0;
offset1=0;
offset3=0;



[files,phi_fox,N2perc]=textread('filename_N2tests.txt','%s %f %f',-1);
RUN_max = length(files);



for RUN=1:RUN_max

[p1,p2,p3,p4,p5,p6]=textread(char(files(RUN)),'%f  %f  %f  %f  %f  %f  %*f
%*f',-1);
time=(1:20000)';

phi_ox = phi_fox(RUN);
N2percent=N2perc(RUN);
s1 = char(files(RUN));
s0 = 'Out_';

outfile = [s0 s1];

pr1=volt2psi*psi2Pa*p1;
```

```
pr3=volt2psi*psi2Pa*p3;
for i=1:20
    offset1 = offset1+pr1(i);
    offset3=offset3+pr3(i);
end
offset1=offset1/20;
offset3=offset3/20;
pr1=pr1-offset1;
pr3=pr3-offset3;

imax = length(pr1);

% Averaging over 5 datapoints
Average = 5;
imax = imax/Average;
for i=1:(imax - 1)
    ps1(i)                                                                    =
(ps1(i)+pr1(5*i+1)+pr1(5*i+2)+pr1(5*i+3)+pr1(5*i+4)+pr1(5*i+5))/Average;
    ps3(i)                                                                    =
(ps3(i)+pr3(5*i+1)+pr3(5*i+2)+pr3(5*i+3)+pr3(5*i+4)+pr3(5*i+5))/Average;
end



for i=0:imax
    ts1(i+1)=Average*i*10^(-6);
    ts3(i+1)=Average*i*10^(-6);
end

figure(1);
plot(ts1,ps1,ts3,ps3);
legend('P1_{smooth}','P3_{smooth}');
xlabel('time (s)');     ylabel('pressure (Pa)');

ps1_max = max(ps1);
ps3_max = max(ps3);

i1_min = find(ps1 == ps1_max);
i3_min = find(ps3 == ps3_max);

ts1_min = ts1(i1_min);
```

```
ts3_min = ts3(i3_min);

imax=length(ps1);
i=1;
while i<(imax-1)
 if ts1(i) > ts1_min
    It_1(i+1)=It_1(i) + 0.5*(ps1(i)+ps1(i+1))*(ts1(i+1)-ts1(i));
 end
 i=i+1;
end

imax=length(ps3);
i=1;
while i<(imax-1)
 if ts3(i) > ts3_min
    It_3(i+1)=It_3(i) + 0.5*(ps3(i)+ps3(i+1))*(ts3(i+1)-ts3(i));
 end
i=i+1;
end
It_1 = A1*It_1;
It_3 = A3*It_3;


% We need to pick the correct It (i.e. the maximum It)

figure(2);
plot(ts1,It_1,ts3,It_3);
legend('I_{T1}','I_{T4}');
xlabel('time (s)');     ylabel('I_T (N-s)');

It_1max = max(It_1);
It_3max = max(It_3);

i1_max = max(find(It_1 == It_1max));
i3_max = max(find(It_3 == It_3max));

ts1_max = ts1(i1_max);
ts3_max = ts3(i3_max);

text(ts1(i1_max),It_1(i1_max),'\leftarrow Max I_{T1}');
```

```
text(ts3(i3_max),It_3(i3_max),'\leftarrow Max I_{T3}');

response = input('Is this correct? 1 = yes, 2 = no: ')

if response ~= 1
   fprintf('Please select the maximum I_T1 ...\n');
   [t_tmp, It_tmp]=ginput(1)

   imax=length(ts1);
   i=1;
   while ts1(i)<t_tmp
         It_1max = It_1(i);
         ts1_max = ts1(i);
         i=i+1;
   end

   fprintf('Please select the maximum I_T3 ...\n');
   [t_tmp, It_tmp]=ginput(1)

   imax=length(ts3);
   i=1;
   while ts1(i)<t_tmp
         It_3max = It_3(i);
         ts3_max = ts3(i);
         i=i+1;
   end
end

It = It_1max + It_3max;

dt1 = ts1_max - ts1_min;
dt3 = ts3_max - ts3_min;

% Small Tube mass calculation

C_N2 = 3*N2percent / (1 - N2percent);

Xox_total = phi_ox + 3 + C_N2;
Xox_fuel = phi_ox/Xox_total;
Xox_O2 = 3/Xox_total;
```

```
Xox_N2 = C_N2/Xox_total;

MW1_mix = Xox_fuel*MW_fuel+Xox_O2*MW_O2 + Xox_N2*MW_N2;
R1_mix = R/MW1_mix;

rho1_mix = Po/(R1_mix*Temp);

Y1_fuel = phi_ox * MW_fuel/(phi_ox * MW_fuel + 3*MW_O2 + C_N2*MW_N2);
Y1_O2 = 3 * MW_O2/(phi_ox * MW_fuel + 3*MW_O2 + C_N2*MW_N2);
Y1_N2 = C_N2*MW_N2/(phi_ox * MW_fuel + 3*MW_O2 + C_N2*MW_N2);

%m1_fuel = m_fuel + m_ox
m1_fuel=(Y1_fuel+Y1_O2)*rho1_mix*Vol_1;

% Large Tube mass calculation

Xair_total=phi_air + 3 + 11.28;             % total number of moles
Xair_fuel = phi_air/Xair_total;             % molar fraction of fuel
Xair_N2 = 11.28/Xair_total;                 % molar fraction of N2
Xair_O2 = 3/Xair_total;                     % molar fraction of O2

MW3_mix = Xair_fuel*MW_fuel+Xair_N2*MW_N2+Xair_O2*MW_O2; % molar weight
of mixture

R3_mix = R/MW3_mix;                         % gas constant of mixture

rho3_mix = Po/(R3_mix*Temp);                % Density of mixture

Y3_fuel = phi_air*MW_fuel/(phi_air*MW_fuel + 3*MW_O2 + 11.28*MW_N2);

m3_fuel=Y3_fuel*rho3_mix*Vol_3;

Ispf=It/((m1_fuel+m3_fuel)*9.81)



fid2=fopen('datalog.txt','a');
fprintf( fid2,'%s \t %f \t %f \t %f \t %f \t %f \t %f \t %f \t %f \t %f
\t %f \t %f \t %f \t %f \n',...
char(files(RUN)), phi_ox, phi_air, N2percent, Temp, m1_fuel, m3_fuel,
ts1_min, ps1_max, ts3_min, ps3_max, dt1, dt3, Ispf);
fclose(fid2);
```

```
fid =fopen(outfile,'w');
fprintf(fid,'phi_ox \t phi_air \t N2p \t Temp \t mf_ox \t mf_air \t ts1_min \t P1max \t ts3_min \t P3max \t DT1 \t DT2 \t Ispf \n');
fprintf(fid,'NA \t NA \t NA \t (K) \t (kg) \t (kg) \t (us) \t (Pa) \t (us) \t (Pa) \t (us) \t (us) \t (s) \n');
fprintf( fid,'%f \t %f \t %f \t %f \t %f \t %f \t %f \t %f \t %f \t %f \t %f \t %f \n\n',...
phi_ox, phi_air, N2percent, Temp, m1_fuel, m3_fuel, ts1_min, ps1_max, ts3_min, ps3_max, dt1, dt3, Ispf);


fprintf(fid,'t1 \t I_T1 \t t3 \t I_T2 \n');
fprintf(fid,'(us) \t (N-s) \t (us) \t (N-s) \n');


for i=1:(imax-1)
    fprintf(fid,'%f \t %f \t %f \n',ts1(i), It_1(i), ts3(i), It_3(i));
end


fclose(fid);
RUN
End
```

THIS PAGE INTENTIONALLY LEFT BLANK

APPENDIX E. TWO-DIMENSIONAL DATA

Two-Dimensional Test Configuration Data																Camera Settings		
Test#	t_fa (s	t_fo (s)	DAQ(N	P_f(p	P_ox(	P_a(p	P_N2	t_p1 (us)	t_p2 (us)	t_p3 (us)	t_p4 (us)	Phi_fo	Phi_fa	N2%	v1 (km/s)	v2 (km/s)	Delay(us)	Width(us)	Gain(V)
031117_1	1.000	4.556	1.000	200	156	534	519	9567	9613	9917	10003	2.1	1.0	55.0%	2.208696	1.772093			
031117_2	1.000	4.556	1.000	200	156	534	519	10741	10787	11088	11176	2.1	1.0	55.0%	2.208696	1.731818			
031117_3	1.000	4.038	1.000	200	160	534	653	3943	3991	4301	4384	2.1	1.0	60.0%	2.116667	1.836145			
031117_4	1.000	4.038	1.000	200	160	534	653	10112	10160	10468	10551	2.1	1.0	60.0%	2.116667	1.836145			
031117_5	1.000	3.371	1.000	200	171	531	868	7021	7068	7374	7459	1.9	1.0	65.0%	2.161702	1.792941			
031117_6	1.000	3.371	1.000	200	171	531	868	8364	8411	8697	8772	1.9	1.0	65.0%	2.161702	2.032			
031117_7	1.000	2.677	1.000	200	188	537	1196	2524	2577	2926	3031	1.8	1.0	70.0%	1.916981	1.451429			
031117_8	1.000	2.677	1.000	200	188	537	1196	2299	2353	2702	2801	1.8	1.0	70.0%	1.881481	1.539394			
031117_9	2.516	0.020	1.000	200	235	537	N/A	7868	7921	8254	8334	1.4	1.0	79.0%	1.916981	1.905			
031117_10	2.516	0.020	1.000	200	235	537	N/A	2603	2657	2987	3068	1.4	1.0	79.0%	1.881481	1.881481			
031117_11	2.516	0.020	1.000	200	235	537	N/A	5672	5727	6057	6139	1.4	1.0	79.0%	1.847273	1.858537			
Transition section 2.5" height, amps set to 100psi/V															#DIV/0!	#DIV/0!			
031118_1	2.454	0.020	1.000	200	237	542	N/A	6364	6418	6751	6835	1.4	1.0	79.0%	1.881481	1.814286			
031118_2	2.454	0.020	1.000	200	237	542	N/A	4830	4884	5220	5303	1.4	1.0	79.0%	1.881481	1.836145			
031118_3	2.454	0.020	1.000	200	237	542	N/A	7079	7133	7470	7552	1.4	1.0	79.0%	1.881481	1.858537			
transition section 2.0" height, amps set to 100psi/V																			
031118_4	2.438	0.020	1.000	200	234	534	N/A	3317	3370	3714	3795	1.4	1.0	79.0%	1.916981	1.881481			
031118_5	2.438	0.020	1.000	200	234	534	N/A	4183	4237	4579	4662	1.4	1.0	79.0%	1.881481	1.836145			
031118_6	2.438	0.020	1.000	200	234	534	N/A	4007	4062	4405	4488	1.4	1.0	79.0%	1.847273	1.836145			
031118_7	1.994	0.020	1.000	200	321	523	N/A	2720	2774	3123	3206	1.0	1.0	79.0%	1.881481	1.836145			
transition section 1.5" height, amps set to 100psi/V																			
031118_8	2.393	0.020	1.000	200	234	534	N/A	4287	4342	4699	4786	1.4	1.0	79.0%	1.847273	1.751724	82	1	700
031118_9	2.393	0.020	1.000	200	234	534	N/A	2625	2679	3057	3139	1.4	1.0	79.0%	1.881481	1.858537	87	1	700
031118_10	2.393	0.020	1.000	200	234	534	N/A	4861	4916	5313	5397	1.4	1.0	79.0%	1.847273	1.814286	92	1	700
031118_11	2.393	0.020	1.000	200	234	534	N/A	3320	3374	3769	3853	1.4	1.0	79.0%	1.881481	1.814286	97	1	700
031118_12	2.393	0.020	1.000	200	234	534	N/A	6811	6866	7263	7344	1.4	1.0	79.0%	1.847273	1.881481	102	1	700
03118_13	2.393	0.020	1.000	200	234	534	N/A	8661	8715	9110	9194	1.4	1.0	79.0%	1.881481	1.814286	107	1	700
transition section 1.0" height, amps set to 100psi/V																			
031119_19	1.000	5.007	1.000	200	148	531	330	7928	7970	8309	8301	2.2	1.0	45.0%	2.419048	-19.05	75	1	700
031119_20	1.000	5.007	1.000	200	148	531	330	3134	3179	3583	3576	2.2	1.0	45.0%	2.257778	-21.77143	65	1	700
031119_21	1.000	5.903	1.000	200	141	531	208	5922	5965	6331	6324	2.3	1.0	35.0%	2.362791	-21.77143	65	1	700
031119_22	1.000	6.556	1.000	200	141	531	128	10072	10114	10487	10464	2.3	1.0	25.0%	2.419048	-6.626087			
031119_23	1.000	4.578	1.000	200	151	529	411	5737	5783	6273	6238	2.2	1.0	50.0%	2.208696	-4.354286			
031119_24	1.000	4.578	1.000	200	151	529	411	5170	5216	5638	5627	2.2	1.0	50.0%	2.208696	-13.85455			
031119_25	1.000	4.088	1.000	200	154	529	514	4357	4404	4906	4897	2.1	1.0	55.0%	2.161702	-16.93333			
031119_26	1.000	4.088	1.000	200	154	529	514	7802	7849	8356	8345	2.1	1.0	55.0%	2.161702	-13.85455			
031119_27	1.000	3.001	1.000	200	171	531	868	7740	7787	8297	8287	1.9	1.0	65.0%	2.161702	-15.24			
031119_28	1.000	3.001	1.000	200	171	531	868	8684	8732	9194	9237	1.9	1.0	65.0%	2.116667	3.544186			
031119_29	1.000	3.001	1.000	200	171	531	868	4932	4981	5404	5481	1.9	1.0	65.0%	2.073469	1.979221			
031119_30	1.000	2.424	1.000	200	185	529	1178	9304	9357	9847	10072	1.8	1.0	70.0%	1.916981	0.677333			
031119_31	1.000	2.424	1.000	200	185	529	1178	7638	7691	8183	8402	1.8	1.0	70.0%	1.916981	0.69589			
031119_32	1.000	2.424	1.000	200	185	529	1178	2256	2309	2802	3018	1.8	1.0	70.0%	1.916981	0.705556			
Moved CH camera upstream to beginning of window																			
031120_1	1.902	0.020	1.000	200	328	534	N/A					1.0	1.0	79.0%			55	1	700
031120_2	1.902	0.020	1.000	200	328	534	N/A					1.0	1.0	79.0%			65	1	700
031120_3	1.902	0.020	1.000	200	328	534	N/A					1.0	1.0	79.0%			75	1	700
031120_4	1.902	0.020	1.000	200	328	534	N/A					1.0	1.0	79.0%			70	1	700
031120_5	1.000	2.946	1.000	200	174	534	881					1.9	1.0	65.0%			70	1	700
031120_6	1.000	2.946	1.000	200	174	534	881					1.9	1.0	65.0%			65	1	700
031120_7	1.000	2.946	1.000	200	174	534	881					1.9	1.0	65.0%			60	1	700
031120_8	1.000	2.946	1.000	200	174	534	881					1.9	1.0	65.0%			55	1	700
Moved CH camera downstream 4.5"																			
031120_9	1.000	2.983	1.000	200	172	534	873					1.9	1.0	65.0%			190	1	700
031120_10	1.000	2.983	1.000	200	172	534	873					1.9	1.0	65.0%			290	1	700
031120_11	1.000	2.983	1.000	200	172	534	873					1.9	1.0	65.0%			210	1	700
031120_12	1.000	2.983	1.000	200	172	534	873					1.9	1.0	65.0%			230	1	700
Shadowgraph imagery																			
031121_1	1.000	2.965	1.000	200	173	537	877	No pressure data				1.9	1.0	79.0%	#VALUE!		55	0.5	700
031121_2	1.000	2.965	1.000	200	173	537	877	7360	7413			1.9	1.0	79.0%	1.916981		60	0.5	700
031121_3	1.000	2.965	1.000	200	173	537	877	8099	8152			1.9	1.0	79.0%	1.916981		60	0.5	700
031121_4	1.000	2.965	1.000	200	173	537	877	8563	8617			1.9	1.0	79.0%	1.881481		60	0.5	700
031121_5	1.000	2.965	1.000	200	173	537	877	10308	10356			1.9	1.0	79.0%	2.116667		65	0.5	700
031121_6	1.000	2.965	1.000	200	173	537	877	7504	7558			1.9	1.0	79.0%	1.881481		65	0.5	700
031121_7	1.000	2.965	1.000	200	173	537	877	6117	6171			1.9	1.0	79.0%	1.881481		65	0.5	700
031121_8	1.000	2.965	1.000	200	173	537	877	No pressure data				1.9	1.0	79.0%	#VALUE!		70	0.5	700
031121_9	1.000	2.965	1.000	200	173	537	877	3145	3199			1.9	1.0	79.0%	1.881481		80	0.5	700
031121_10	1.000	6.000	1.000	200	143	537	210	4939	4982			2.3	1.0	35.0%	2.362791		55	0.5	700
031121_11	1.000	6.000	1.000	200	143	537	210	8109	8152			2.3	1.0	35.0%	2.362791		65	0.5	700
031121_12	1.000	6.000	1.000	200	143	537	210	5440	5481			2.3	1.0	35.0%	2.478049		65	0.5	700
031121_13	1.000	6.000	1.000	200	143	537	210	3438	3481			2.3	1.0	35.0%	2.362791		65	0.5	700
031121_14	1.000	6.000	1.000	200	143	537	210	5451	5493			2.3	1.0	35.0%	2.419048		75	0.5	700
031121_15	1.000	6.000	1.000	200	143	537	210	7829	7871			2.3	1.0	35.0%	2.419048		80	0.5	700

Table 4. Two-Dimensional Test Configuration Data

THIS PAGE INTENTIONALLY LEFT BLANK

APPENDIX F. CH* IMAGERY

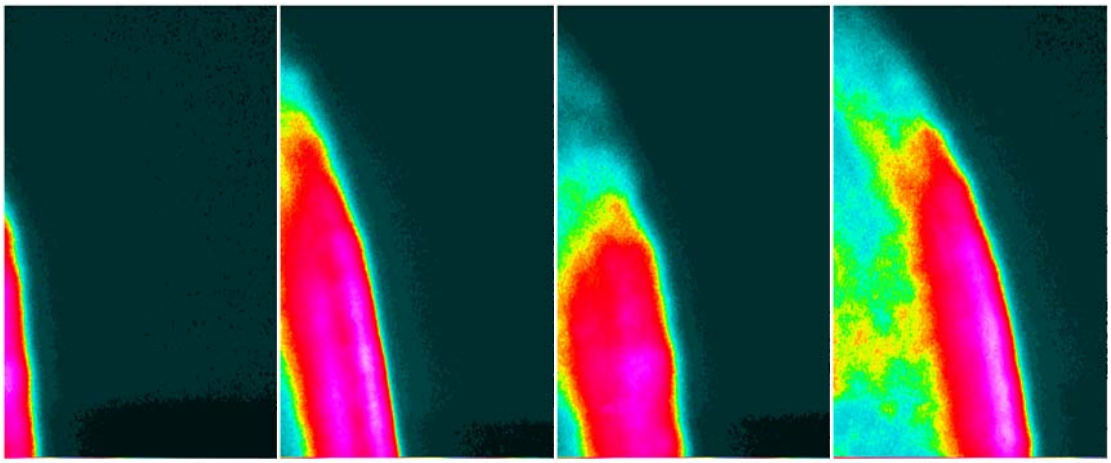

64 μs 66 μs 68 μs 70 μs

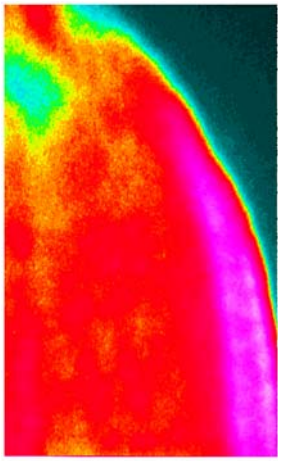

72 μs

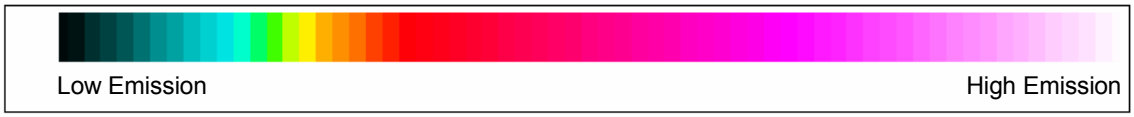

Figure 43 CH* Images with Area Ratio of 1.33 and 35% N_2 Dilution

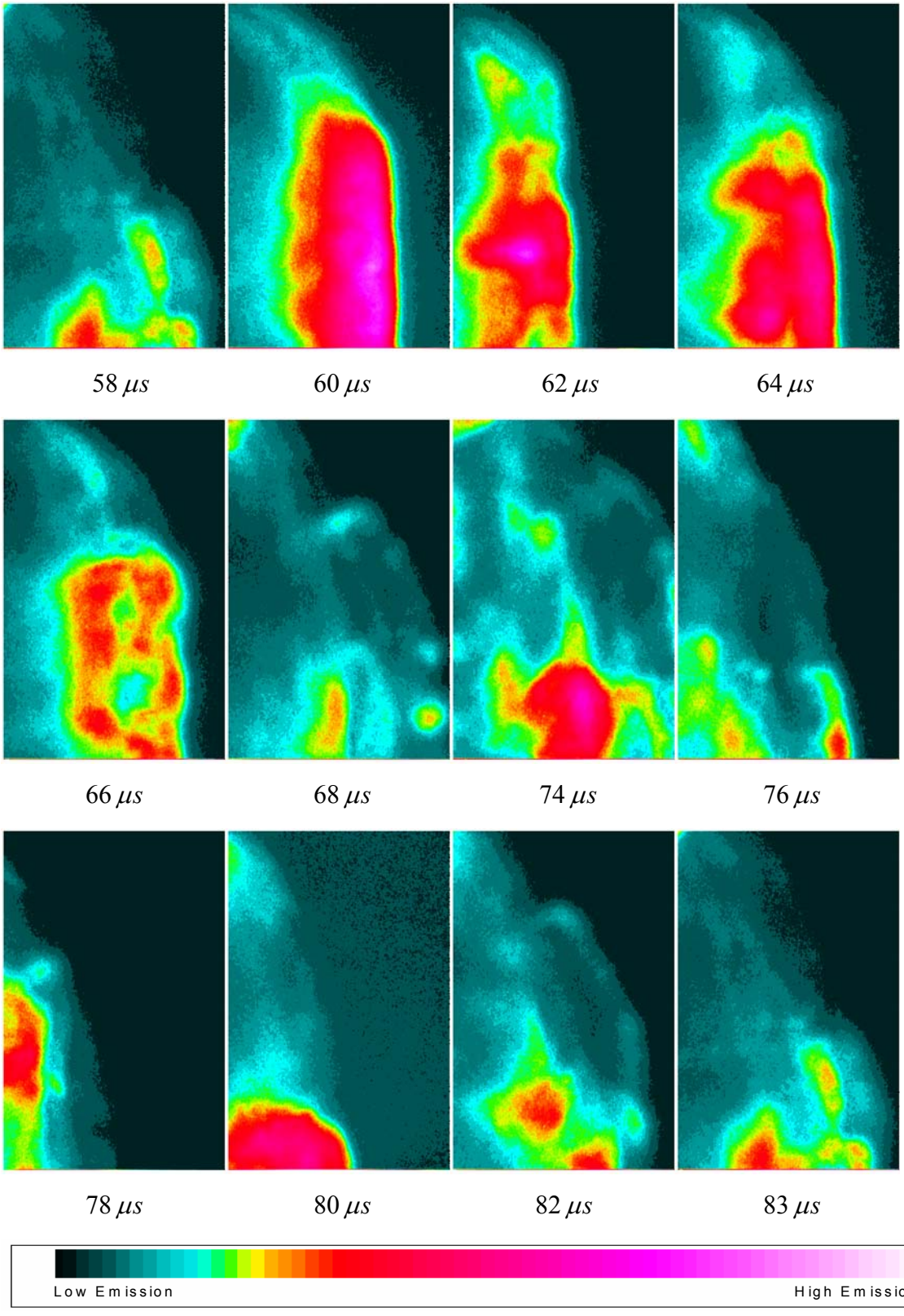

Figure 44 CH* Images with Area Ratio of 1.33 and 55% N_2 Dilution

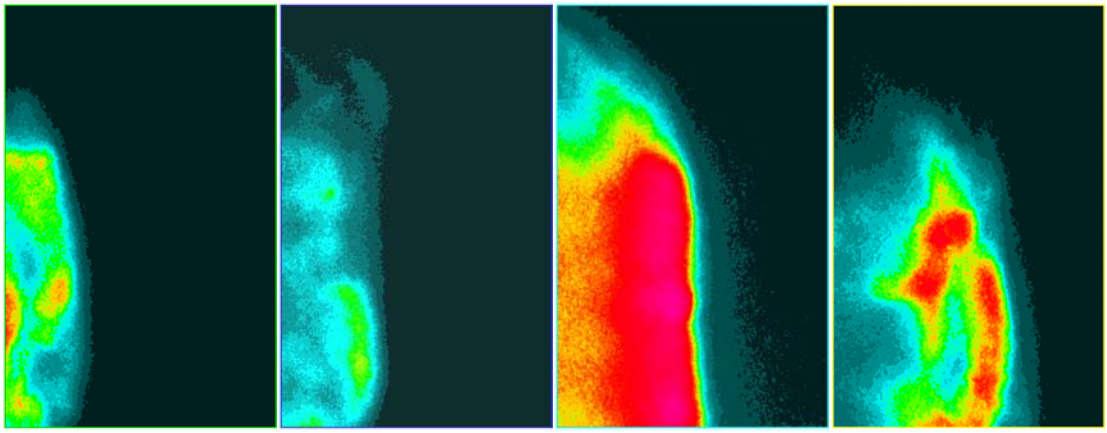

64 μs 66 μs 68 μs 70 μs

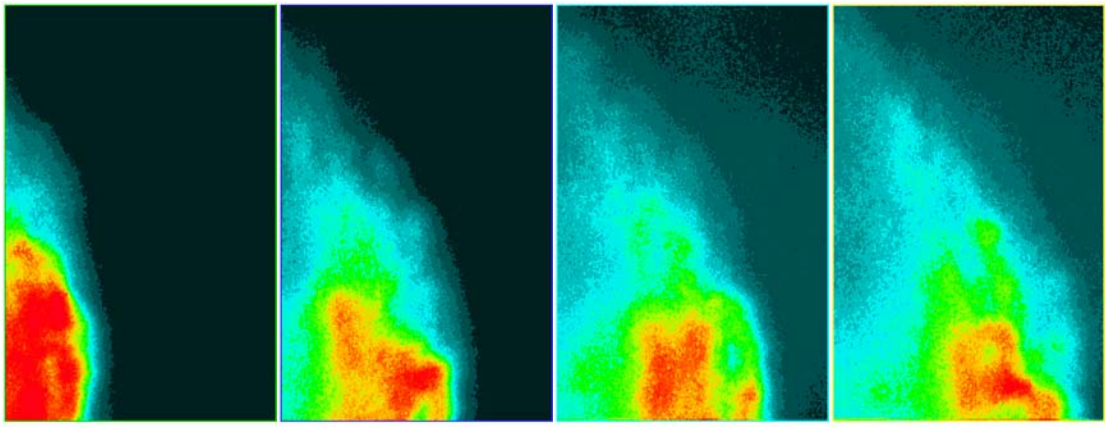

82 μs 86 μs 88 μs 90 μs

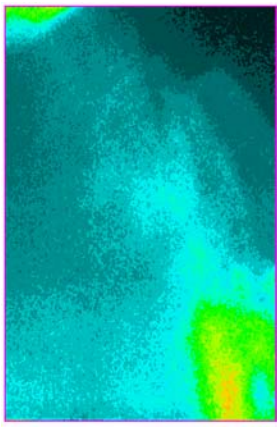

95 μs

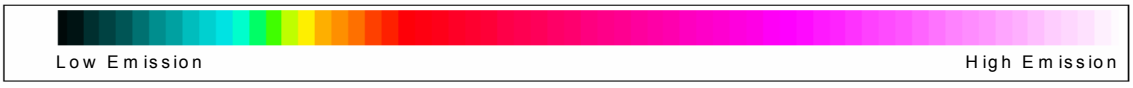

Figure 45 CH* Images with Area Ratio of 1.33 and 79% N_2 Dilution

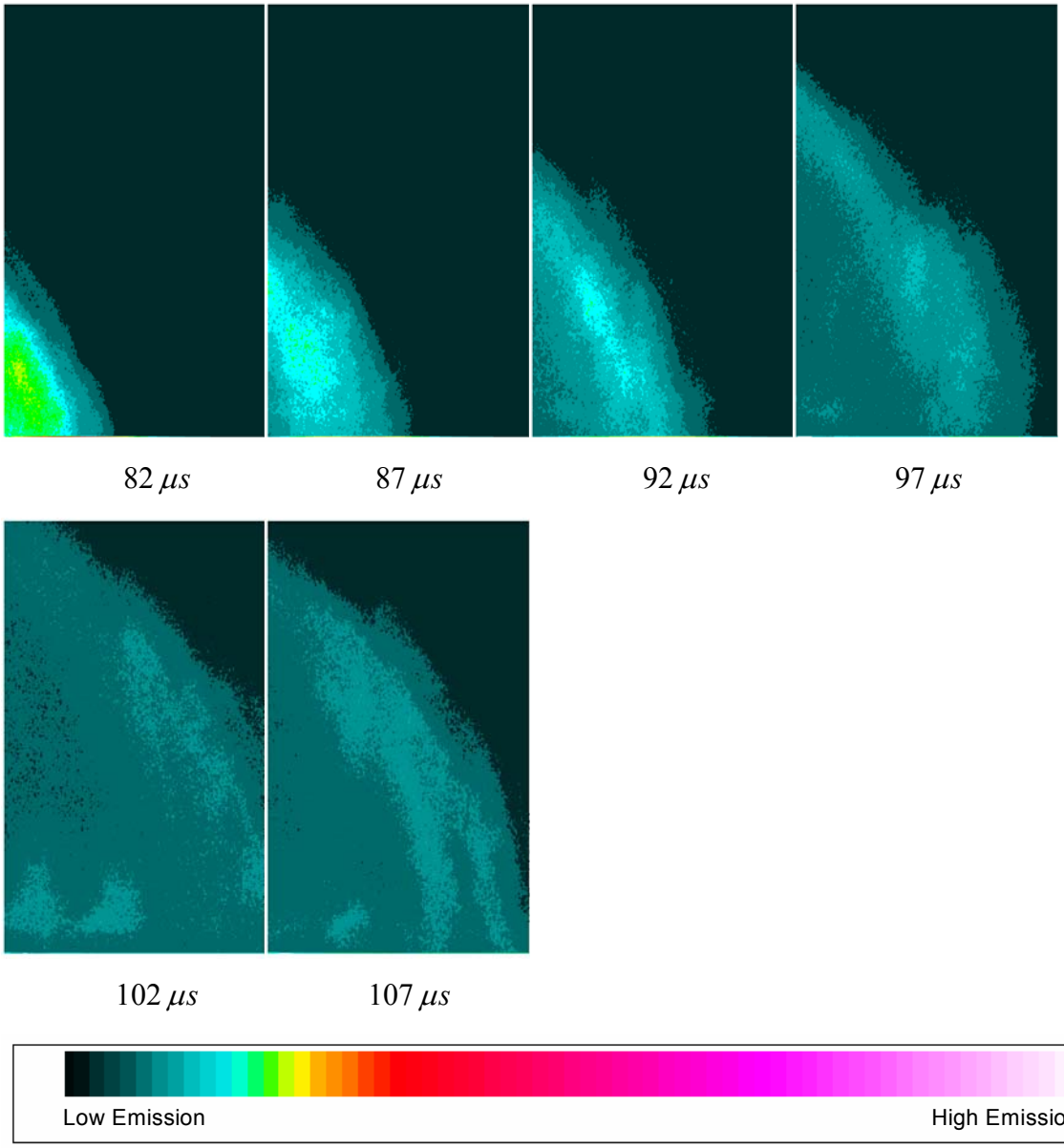

Figure 46 CH* Images with Area Ratio of 2.67 and 79% N_2 Dilution

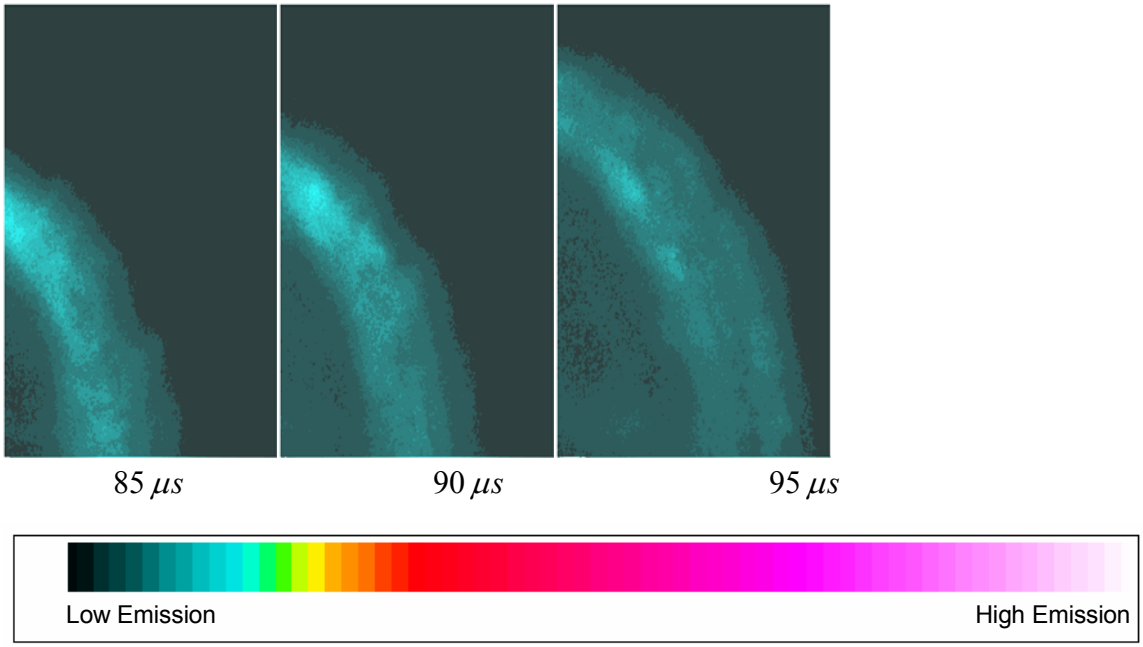

Figure 47 CH* Images with Area Ratio of 4.0 and 50% N_2 Dilution

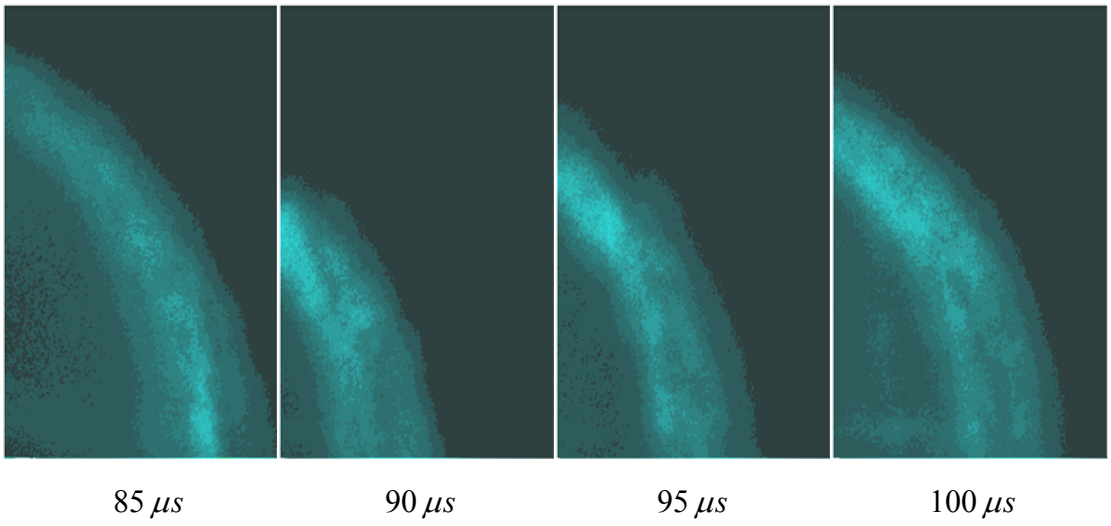

Figure 48 CH* Images with Area Ratio of 4.0 and 55% N_2 Dilution

THIS PAGE INTENTIONALLY LEFT BLANK

LIST OF REFERENCES

[1] Hofstedt, T.A., "Propagation of a Two-Phase Detonation Across a Geometric Diffraction with Compositional Discontinuity," Master's Thesis, U.S. Naval Postgraduate School, Monterey, CA, June 2000.

[2] Kelly, Jim. "After Combustion: Detonation!" *Popular Science.* pp. 51-58, 115, September 2003.

[3] Brophy, C.M., Sinibaldi, J.O., Netzer, D., and Kailasanath, K., "Initiator Diffraction Limits in a Pulse Detonation Engine," Moscow, Russia, 2000.

[4] Kuo, K.K., *Principles of Combustion,* John Wiley & Sons, Inc., 1986.

[5] Glassman, I., *Combustion*, Academic Press, Inc., 1987.

[6] Li, Chiping, and Kailasanath K., "Detonation Diffraction in Pulse Detonation Engines," AIAA Paper 2000-3470, 36th AIAA/ASME/SAE/ASEE Joint Propulsion Conference and Exhibit, Huntsville, AL, 16-19 July 2000.

[7] Brophy, C.M., Werner, S., and Sinibaldi, J.O., "Performance Characterization of a Valveless Pulse Detonation Engine," AIAA Paper 2003-1344, 41st AIAA Aerospace Sciences Meeting & Exhibit, Reno, NV, 6-9 January 2003.

[8] Teodorczyk, A., Lee, J.H.S., and Knystautas, R., "Photographic Study of the Structure of Propagation Mechanisms of Quasidetonations in Rough Tubes," Progress in Astronautics and Aeronautics, Vol. 133, AIAA, New York, NY, 1990, pp. 223-240.

[9] Oran, E.S., and Boris, J.P., "Ignition in a Complex Mach Structure," Progress in Astronautics and Aeronautics, Vol. 153, AIAA, New York, NY, 1993, pp. 241-252.

[10] Murray, S.B., Zhang, F., and Gerrard, K.B., "The Influence of Driver Power and Receptor Confinement on Pre-detonators for Pulse Detonation Engines," 18th International Colloquium on the Dynamics of Explosions and Reactive Systems, Seattle, WA, 10-12 August 2001.

[11] Murray, S.B., and Lee, J.H., "On the Transformation of Planar Detonation to Cylindrical Detonation," *Combustion and Flame*, Vol. 52, pp. 269, 1983.

[12] Desbordes, D., "Transmission of Overdriven Plane Detonations: Critical Diameter as a Function of Cell Regularity and Size," Progress in Astronautics and Aeronautics, Vol. 114, AIAA, New York, NY, 1988, pp. 170-185.

[13] Desbordes, D., and Lannoy, A., "Effects of a Negative Step of Fuel Concentration on Critical Diameter of Diffraction on a Detonation," Progress in Astronautics and Aeronautics, Vol. 133, AIAA, New York, NY, 1990, pp. 170-186.

[14] Brophy, C.M., Sinibaldi, J.O., and Damphousse, P., "Initiator Performance for Liquid-Fueled Pulse Detonation Engines," AIAA Paper 2002-0472, 40th AIAA Aerospace Sciences Meeting & Exhibit, Reno, NV, 14-17 January 2002.

[15] Bussing, T.R.A., Bratkovich, and T.E., Hinkey Jr., J.B., "Practical Implementation of Pulse Detonation Engines," AIAA Paper 97-2748, 33rd AIAA/ASME/SAE/ASEE Joint Propulsion Conference and Exhibit, Seattle, WA, 6-9 July 1997.

[16] Kailasanath, K., "On the Performance of Pulsed Detonation Engines," International Colloquium on Advances in Confined Detonation, Moscow, Russia, 2-5 July 2002.

[17] Settles, G.S., *Schlieren and Shadowgraph Techniques*. Springer, 2001.

[18] Fludovich Jr., M. A., "Investigation of Detonation Wave Diffraction Interaction with Reactive Transpiration," Master's Thesis, U.S. Naval Postgraduate School, Monterey, CA, September 2002.

INITIAL DISTRIBUTION LIST

1. Defense Technical Information Center
   Ft. Belvoir, Virginia

2. Dudley Knox Library
   Naval Postgraduate School
   Monterey, California

3. Christopher M. Brophy
   Department of Mechanical and Astronautical Engineering
   Naval Postgraduate School
   Monterey, California

4. Jose O. Sinibaldi
   Naval Postgraduate School
   Department of Mechanical and Astronautical Engineering
   Monterey, California